

Colloquium: Majorana Fermions in nuclear, particle and solid-state physics

Steven R. Elliott*

Los Alamos National Laboratory, Los Alamos, NM, USA, 87545

Marcel Franz†

Department of Physics and Astronomy, University of British Columbia, Vancouver, BC, Canada, V6T 1Z1

Ettore Majorana (1906-1938) disappeared while traveling by ship from Palermo to Naples in 1938. His fate has never been fully resolved and several articles have been written that explore the mystery itself. His demise intrigues us still today because of his seminal work, published the previous year, that established symmetric solutions to the Dirac equation that describe a fermionic particle that is its own anti-particle. This work has long had a significant impact in neutrino physics, where this fundamental question regarding the particle remains unanswered. But the formalism he developed has found many uses as there are now a number of candidate spin- $\frac{1}{2}$ neutral particles that may be truly neutral with no quantum number to distinguish them from their anti-particles. If such particles exist, they will influence many areas of nuclear and particle physics. Most notably the process of neutrinoless double beta decay can only exist if neutrinos are massive Majorana particles. Hence, many efforts to search for this process are underway. Majorana's influence doesn't stop with particle physics, however, even though that was his original consideration. The equations he derived also arise in solid state physics giving rise to emergent states that are described as Majorana fermions. Our theoretical understanding indicates that such states must exist in superconductors and, in fact, there is some evidence that they have been observed. If so, it might lead to advances in quantum computing. This review first summarizes the basics of Majorana's theory and its implications. It then provides an overview of the rich experimental programs trying to find a fermion that is its own anti-particle in nuclear, particle, and solid state physics.

Contents

I. Introduction	1
A. The Particle Physics View	2
B. The Solid State Physics View	3
C. Significance and potential applications	4
II. Majorana fermions in nuclear and particle physics	4
A. The Majorana-Dirac Equations	5
B. The Seesaw Mechanism	5
C. Lepton Number Conservation	6
D. Leptogenesis	6
E. Double Beta Decay	7
F. Supersymmetry	8
III. Majorana fermions in solid state devices	9
A. Majorana fermions as emergent particles in topological superconductors	9
1. General considerations	9
2. Majorana zero modes	11
B. Kitaev chain: the 1D prototype system	13
C. Physical realizations in 1D	15
1. Edge of a 2D topological insulator	15
2. Nanowire made from a 3D topological insulator	16
3. Semiconductor quantum wires	17
4. Helical spin chains	18
D. Systems in two dimensions	19
1. Non-Abelian exchange statistics: general considerations	19
2. Vortices in Fu-Kane model	20
3. Vortex exchange and braiding	21

IV. Prospects for Observation	23
A. Prospects in nuclear and particle physics	23
1. Double beta decay	23
2. Accelerator Searches	26
3. Searches for a Fourth Neutrino	26
4. Dark Matter Searches	27
B. Observations in solid state devices	28
1. Quantum wires and other 1D systems	30
2. 2D systems	31
V. Summary and conclusions	31
Acknowledgments	32
References	32

I. INTRODUCTION

In the late 1920's Schrödinger published his non-relativistic wave equation (Schrödinger, 1926) describing the quantum behavior of fundamental particles. Soon thereafter Paul Dirac developed the wave equation (Dirac, 1928) that bears his name describing the behavior of relativistic particles. About a decade later, Ettore Majorana recognized the importance of a specific representation of the Dirac Equation (Majorana, 1937). There are numerous examples of physical quantities that are described by the Dirac Equation, but as yet, none have been found that obey that of Majorana. Discovering particles or quasi-particles that are governed by Majorana's formalism would have significant implications for science ranging from cosmology to particle physics to solid state physics. The remarkable achievement of the

*Electronic address: elliotts@lanl.gov

†Electronic address: franz@physics.ubc.ca

Majorana Equation and its potential consequences motivate this colloquium.

A. The Particle Physics View

Schrödinger's Equation was developed using the classical equation relating energy (E) to momentum (p) for a particle of mass m

$$E = p^2/2m, \quad (1)$$

and substituting the corresponding differential operators:

$$\begin{aligned} E &\rightarrow i\frac{\delta}{\delta t} \\ \mathbf{p} &\rightarrow i\nabla \end{aligned} \quad (2)$$

to find the resulting wave equation,

$$i\dot{\psi} = \frac{1}{2m}\nabla^2\psi \quad (3)$$

where ψ is the wavefunction. Relativistically, the energy-momentum relation is

$$E^2 = p^2 + m^2 \quad (4)$$

and a straight-forward substitution of the operators leads to the Klein-Gordon equation which has a double differentiation with respect to time. This characteristic, unlike the Schrödinger Equation, means that the probability of the value of a dynamic variable cannot be predicted at a future time when ψ is provided at a given earlier time.

Dirac, wanting to avoid this feature, succeeded in writing an equation that was linear in $\dot{\psi}$, removing this difficulty. Dirac wrote his equation as

$$i\dot{\psi} = (\boldsymbol{\alpha} \cdot \mathbf{p} + \beta m)\psi. \quad (5)$$

The α 's and β of Eq. 5 do not commute and hence they cannot be simple numbers, but Dirac was able to find a set of 4×4 matrices that met the requirements for his equation. The solutions of Eq. 5 are 4-component vectors that describe a spin- $\frac{1}{2}$ particle that is distinct from its anti-particle. Such particles, including the electron and neutron, were found soon after Dirac's publication, and his work has been considered a prediction of their existence.

A more modern description expresses the Dirac equation so that it is manifestly Lorentz covariant. One can write Eq. 5 as such by multiplying the equation by the matrix β and defining the Dirac representation matrices $\gamma^\mu = (\beta; \beta\alpha_i)$. The equation is then

$$(i\gamma^\mu\delta_\mu - m)\psi = (\gamma^\mu p_\mu - m)\psi = 0. \quad (6)$$

Note that $p^\mu = (E, \mathbf{p})$, $p_\mu = (E, -\mathbf{p})$ and δ_μ is shorthand for $\frac{\partial}{\partial x^\mu}$. The explicit form of the Dirac matrices can be written in terms of the 2x2 Pauli matrices (σ^i),

$$\sigma^1 = \begin{pmatrix} 0 & 1 \\ 1 & 0 \end{pmatrix}, \sigma^2 = \begin{pmatrix} 0 & -i \\ i & 0 \end{pmatrix}, \sigma^3 = \begin{pmatrix} 1 & 0 \\ 0 & -1 \end{pmatrix}, \quad (7)$$

and σ^0 is the identity matrix. Denoting $\sigma^\mu = (\sigma^0, -\sigma^i)$ and $\hat{\sigma}^\mu = (\sigma^0, \sigma^i)$, the Dirac matrices can be written, in the Weyl Representation, as;

$$\gamma^\mu = \begin{pmatrix} 0 & \sigma^\mu \\ \hat{\sigma}^\mu & 0 \end{pmatrix} = \begin{pmatrix} \begin{bmatrix} 0 & 0 & 1 & 0 \\ 0 & 0 & 0 & 1 \\ 1 & 0 & 0 & 0 \\ 0 & 1 & 0 & 0 \end{bmatrix}, \begin{bmatrix} 0 & 0 & 0 & -1 \\ 0 & 0 & -1 & 0 \\ 0 & 1 & 0 & 0 \\ 1 & 0 & 0 & 0 \end{bmatrix}, \begin{bmatrix} 0 & 0 & 0 & i \\ 0 & 0 & -i & 0 \\ 0 & -i & 0 & 0 \\ i & 0 & 0 & 0 \end{bmatrix}, \begin{bmatrix} 0 & 0 & -1 & 0 \\ 0 & 0 & 0 & 1 \\ 1 & 0 & 0 & 0 \\ 0 & -1 & 0 & 0 \end{bmatrix} \end{pmatrix}. \quad (8)$$

The choice of the matrices in Eq. 8, however, is not unique. Majorana's insight was that for a particular choice of the α 's and β , Eq. 5 is real with a real solution. The Dirac equation is actually four coupled equations for 4 spinor components. For the Majorana equation, the condition of reality reduces this to two independent systems, each with two coupled equations. The solution to one of these systems then describes a truly neutral particle, still spin $\frac{1}{2}$, but with no distinction between particle and anti-particle. Such a particle, if found, would be termed a Majorana fermion.¹ Eddington (Eddington,

1928) noted that one could derive symmetrical equations from the Dirac equation, but it was Majorana who noted the particle/anti-particle correspondence and its importance for neutrinos.

The four components of a Dirac wave function describe a particle and anti-particle pair, each with spin $\frac{1}{2}$. The equivalent in the Majorana picture are two particles, each of spin $\frac{1}{2}$. In some sense one can consider a Dirac fermion

¹ Majorana's paper was published a year before his disappearance

from a transport ship between Palermo and Naples. The story behind his life and theories of his demise are interesting in their own right and are summarized by Holstein (Holstein, 2009) and references therein.

as a special case of a Majorana fermion pair. Two, mass-degenerate Majorana fermions with opposite CP parity² would be indistinguishable from a Dirac fermion with that same mass.

In both pictures, if these particles were massless, their spin would always lie parallel (right handed) or anti-parallel (left handed) to their direction of motion. Since they do have mass, however, they are never in a pure helicity state but possess a component of the other helicity in proportion to the mass. Figure 1 shows this relationship for neutrinos, which will become important in the discussion of the attempts to find Majorana fermions.

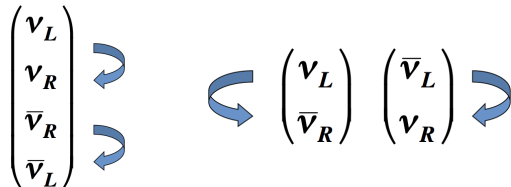


FIG. 1 A non-zero mass will mix helicities for a particle with spin. The left panel shows a 4-component spinor for a Dirac neutrino. ν_R (ν_L) indicates a right (left) handed neutrino. $\bar{\nu}_R$ ($\bar{\nu}_L$) indicates a right (left) handed anti-neutrino. The arrows indicate which states are mixed due to the presence of mass. The right panel shows a similar description but for the two Majorana particles. In this case, the bars indicating anti-particles are superfluous and are only used to help the reader connect the states between the two cases.

B. The Solid State Physics View

In solid state physics the only fermionic particles that matter for all practical purposes are electrons. Electrons are, of course, Dirac fermions. However, as it turns out, Majorana fermions can occur in certain solids as *emergent quasiparticles* which can be thought of as collective excitations of the quantum many-body state describing the interacting electron system.

Condensed matter physics is replete with examples of emergence (Anderson, 1972). Emergent particles in solids range from those very well established (phonons, magnons, plasmons, polarons) through some that are more elusive (triplons, composite fermions) to truly exotic and speculative (spinons, holons, chargons, visons, etc.). At the conventional end, phonons for example represent quanta of the lattice vibrations, and form an essential ingredient in the description of the low-temperature thermodynamic and transport properties of all solids (Kittel, 1987). Magnons – quanta of spin fluctuations

– are similarly essential in the description of magnetic solids, as are polarons for ionic insulators and semiconductors. In this sense, emergent particles are as real as the elementary particles in nuclear and high-energy physics. Observation of an emergent Majorana fermion in a solid state system would be as exciting, and perhaps even more so, as establishing that e.g. the neutrino is a Majorana fermion. As we shall see in Sec. III solid state physics may in fact be very close to this goal with many experts of the opinion that a Majorana fermion has already been observed in semiconductor quantum wires.

To understand how Majorana fermions emerge in a system comprised of many electrons we must first briefly review the structure of such electronic many-body states. These are efficiently described using the formalism of second quantization which is uniquely suited to handle systems with a very large numbers of identical particles in condensed matter physics. In this formalism electrons are represented by a set of creation and annihilation operators where c_j^\dagger creates an electron with quantum numbers denoted by index j while c_j annihilates it. In a typical situation j includes the position degree of freedom as well as the orbital and spin quantum numbers. As appropriate for identical fermions these operators obey the canonical anticommutation relations

$$\begin{aligned} \{c_i^\dagger, c_j^\dagger\} &= \{c_i, c_j\} = 0, \\ \{c_i^\dagger, c_j\} &= \delta_{ij}. \end{aligned} \quad (9)$$

A Hamiltonian describing electrons in an arbitrary solid can be expressed in terms these operators; the electron kinetic energy will be represented by terms bi-linear in c 's while interactions will contain quartic terms.

Without any loss of generality, one can perform a canonical transformation of the Hamiltonian (and any other operator of interest) to the “Majorana basis”,

$$c_j = \frac{1}{2}(\gamma_{j1} + i\gamma_{j2}), \quad c_j^\dagger = \frac{1}{2}(\gamma_{j1} - i\gamma_{j2}), \quad (10)$$

where the new operators $\gamma_{j\alpha}$, which can be loosely thought of as the real and the imaginary part of the electron operator, satisfy the following algebra

$$\{\gamma_{i\alpha}, \gamma_{j\beta}\} = 2\delta_{ij}\delta_{\alpha\beta}, \quad \gamma_{i\alpha}^\dagger = \gamma_{i\alpha}. \quad (11)$$

The last relation informs us that a particle created by the γ -operator is identical to its antiparticle: creating and destroying such a particle has the same effect on the state of the system. This is a Majorana fermion.

The above discussion shows that *any* system of electrons can be formally recast in terms of Majorana fermion operators through the canonical transformation (10,11). In most cases, however, such a transformation brings no benefit and merely complicates things. Physically this is because in most cases the two Majoranas comprising a given electron are intertwined in space and it thus makes little sense to describe them as separate entities. There is,

² When the operator CP acts upon a wave function, it changes the sign of all the position coordinates and changes the particle to anti-particle. For a Majorana fermion it is somewhat more subtle as $C^2|\nu\rangle \equiv |\nu\rangle$, and therefore $CP|\nu\rangle = \pm i|\nu\rangle$ (Carruthers, 1971; Kayser and Goldhaber, 1983)

however, a special class of systems, called topological superconductors, in which two Majorana fermions comprising a single electron become spatially separated. In this case a description through the Majorana basis becomes compulsory as no other basis can accurately account for the true physical degrees of freedom in the system. It is precisely this class of systems that we will discuss in great detail in Sec. III since they exhibit, in very real and quantifiable sense, independent Majorana particles.

There are a number of conditions that must be satisfied for a system of electrons to exhibit unpaired Majorana fermions. One key condition that can be easily understood follows immediately from inverting the transformation specified in Eq. (10) to obtain

$$\gamma_{j1} = c_j^\dagger + c_j, \quad \gamma_{j2} = i(c_j^\dagger - c_j). \quad (12)$$

These relations reveal that isolated Majorana fermions can only be found in systems with superconducting order. This is because coherent superpositions of electron and hole degrees of freedom, indicated in Eqs. (12), are known to naturally occur only in the theory of superconductivity, originally due to Bardeen, Cooper and Schrieffer (Bardeen *et al.*, 1957). Also, an operator defined in Eq. (12) can only act nontrivially on a ground state with uncertain total number of particles; such a ground is characteristic of superconducting systems. It therefore follows that one needs a superconductor to observe Majorana fermions in the solid-state context but it should be noted that only a certain special type of superconductor will exhibit this behavior. We will discuss below the additional conditions that must be met in order to obtain the requisite ‘topological’ superconductor.

Whether or not a neutrino (or another elementary particle) is a Majorana fermion remains ultimately an experimental question: theory allows such a possibility but experiment will have the final word. In solid state physics the situation is somewhat different. The relevant theory, based on the band theory of solids and the BCS theory of superconductivity, both exceptionally well understood and tested, unambiguously predicts Majorana fermions. There is no doubt that Majorana fermions should emerge in suitable systems under specific, precisely defined conditions. The uncertainty has to do with the question of whether or not the experiments have achieved these conditions. Further uncertainty arises from the difficulties related to the unambiguous detection of the Majorana particle in a solid-state device, where its signatures can be masked by the effect of disorder or mimicked by other unrelated effects. At the time of this writing a consensus is building up that Majorana particles have been observed in recent experiments on semiconductor quantum wires proximity-coupled to a superconductor (Mourik *et al.*, 2012). Experiments on other systems that have been proposed to host Majorana particles are being actively pursued. In Sec. III we shall review the underlying theory and describe the relevant experimental work as well as discuss in more detail various uncertainties that still exist.

C. Significance and potential applications

The broad interest in the physics community regarding the existence of Majorana states, whether they be true particles or an emergent quantum state in condensed matter systems, arises because of the significance of such states and their potential applications. Here we mention two important potential outcomes of the existence of Majorana fermions: leptogenesis and quantum computing.

Observationally, the Universe is composed of matter with no, or little, anti-matter. This fact is necessary for us to exist in order to even ponder it. There must have been an initial imbalance between the two, or otherwise all matter would have annihilated with anti-matter leaving nothing to form the galaxies, solar systems, planets and, of course, us. The Big Bang, however, made an equal number of matter and anti-matter particles at the Universe’s beginning. The final asymmetry between matter and anti-matter arose dynamically after the Big Bang. If neutrinos are Majorana particles, the theory of leptogenesis might explain this asymmetry. We discuss this possibility in Sec. II.D.

In a solid state system, Majorana fermions naturally appear in superconducting systems and can appear isolated and unpaired in topological superconductors. The state vector that describes such fermions that are spatially separated can be used to encode quantum information. Since the fermions are spatially separated, the information in each quantum bit is stored nonlocally leading to long decoherence times, a necessary feature for quantum computing. We discuss this possibility in Sec. III.D.1.

II. MAJORANA FERMIONS IN NUCLEAR AND PARTICLE PHYSICS

The neutrino is the *usual suspect* when one discusses fundamental particles that might be Majorana in nature. The neutrino only interacts weakly and therefore it is very difficult to observe its behavior. As a result, there are key aspects of the neutrino, such as its mass, that are still unknown. Furthermore, the weak interaction violates parity and therefore right-handed neutrinos (and left handed anti-neutrinos) have no interaction. Therefore, it is unknown if those states are unobservable or simply don’t exist. The quantum mechanics of neutrinos, be they Dirac or Majorana particles, has been described in detail in many places. (See for example Refs. (Boehm and Vogel, 1987; Kayser, 1989; Mohapatra and Pal, 1991) and (Zralek, 1997).) Here we provide an overview.

A. The Majorana-Dirac Equations

The solution of the free-particle Dirac Equation (Eq. 6) is a four-component bi-spinor,

$$\Psi = \begin{pmatrix} \psi_1 \\ \psi_2 \\ \psi_3 \\ \psi_4 \end{pmatrix}. \quad (13)$$

If the spin vector of a particle points in the same direction as its momentum, it is referred to as right-handed. Defining ψ_R and ψ_L as the two component spinors that are the right-handed and left-handed projections of ψ (chiral projections),

$$\Psi \equiv \begin{pmatrix} \psi_R \\ \psi_L \end{pmatrix}, \quad (14)$$

we can write the Dirac Equation,

$$\begin{aligned} (E - \mathbf{p} \cdot \boldsymbol{\sigma})\psi_R - m_D\psi_L &= 0 \\ (E + \mathbf{p} \cdot \boldsymbol{\sigma})\psi_L - m_D\psi_R &= 0, \end{aligned} \quad (15)$$

where we have suggestively added a subscript D for Dirac to the mass (m_D).

We noted in Sec. I.A that if a set of γ 's are found that makes the Dirac equation real, then the solutions are real resulting in the Majorana condition that ψ and its CP partner are identical. Majorana realized this possibility by finding purely imaginary versions of the γ 's resulting in a representation of the Dirac equation that is real. One can express the wave functions in any representation of the Dirac matrices once they are found, and so to compare more easily, we will continue with the Weyl (or chiral) representation. In this representation (Eq. 8), the definition of a Majorana field can be written as the transformation³: $\Psi_{L(R)}^c = i\gamma^2\gamma^0\bar{\Psi}_{L(R)}^T$, where the operator CP in this representation is given by $i\gamma^2\gamma^0$; however, some authors state the Majorana definition with only the operator C : $\Psi = i\gamma^2\Psi^*$. Putting all this together, the ³ $\bar{\Psi}$ is the adjoint of Ψ given by $\Psi^\dagger\gamma^0$, where the \dagger indicates the conjugate transpose and T indicates the simple transpose.

corresponding Majorana version of the equations are

$$\begin{aligned} (E - \mathbf{p} \cdot \boldsymbol{\sigma})\psi_R - im_R\sigma_2\psi_R^* &= 0 \\ (E + \mathbf{p} \cdot \boldsymbol{\sigma})\psi_L - im_L\sigma_2\psi_L^* &= 0. \end{aligned} \quad (16)$$

Here we have explicitly indicated that the masses are not required to be equal since the Majorana Equation decouples. This is not so for the Dirac Equation. One should recognize that when the mass is zero, the two equations are equivalent. Also note that if a pair of Majorana particles have equal masses but opposite CP parity, that pair would be indistinguishable from a Dirac particle. The two fields ψ_L and ψ_R are both eigenstates of CP with opposite eigenvalues or CP parities.

The Majorana fields can be expressed in 4-component form as

$$\Psi_L = \begin{pmatrix} -i\sigma_2\psi_L^* \\ \psi_L \end{pmatrix}, \Psi_R = \begin{pmatrix} \psi_R \\ i\sigma_2\psi_R^* \end{pmatrix}. \quad (17)$$

From this expression, it can be seen that a pair of Majorana fields with $m_L = m_R$ and $\psi_L = i\sigma_2\psi_R^*$ is equivalent to a Dirac Field. This 4-component form will be of use in understanding the different issues concerning mass in the following section.

B. The Seesaw Mechanism

In field theory, the wave equations given by Eqns. 15 and 16 can be derived from a Lagrangian density (\mathcal{L}) using a variational principle (the Euler-Lagrange equation). The appropriate \mathcal{L} includes mass terms (\mathcal{L}_{mass}) whose form would depend on whether the particles were described as Majorana or Dirac. In the case of neutrinos, for example, it is not known which type they are so in principle both possibilities should be considered. Although there are 3 flavors of neutrino, it is instructive to look at \mathcal{L}_{mass} for a lone flavor. Hence the mass terms of \mathcal{L}_{mass} are written:

$$\begin{aligned} \mathcal{L}_{mass} &= m_D[\bar{\nu}_R\nu_L + (\bar{\nu}_L)^c\nu_R^c] + m_L[(\bar{\nu}_L)^c\nu_L + \bar{\nu}_L\nu_L^c] + m_R[(\bar{\nu}_R)^c\nu_R + \bar{\nu}_R\nu_R^c] \\ &= -\frac{1}{2}(\bar{\nu}_L)^c \begin{pmatrix} \nu_R \\ \nu_R^c \end{pmatrix} \begin{pmatrix} m_L & m_D \\ m_D & m_R \end{pmatrix} \begin{pmatrix} \nu_L \\ (\nu_R^c)^c \end{pmatrix} \end{aligned} \quad (18)$$

where we have introduced the notation $\nu_{R,L}$ for the respective neutrino annihilation operators replacing the generic $\Psi_{R,L}$ notation of Eq. 17. With the possibility that all three mass terms exist, \mathcal{L}_{mass} must be diagonalized resulting in two mass eigenvalues. In the seesaw

model (Gell-Mann *et al.*, 1979; Yanagida, 1979), the assumption is made that m_R is very large compared to m_D and m_L is zero. This was motivated by the non-observation of ν_R , which can be explained if its mass is very heavy. It also seems natural that m_D should

have a value near that of the charged fermions (e.g. the electron). Under these assumptions, diagonalizing the matrix one finds that the two eigenvalues are m_R and $m_\nu \sim m_D^2/m_R$. It's critical to notice here that m_ν is much smaller than the typical charged Dirac lepton, which agrees with an important empirical fact. Equally important is that we have 2 Majorana neutrinos. This seesaw mechanism not only provides a hint as to why neutrino masses are so small but also ties that hint to the character of neutrinos being Majorana.

C. Lepton Number Conservation

Empirically, no process has been observed that changes the total number of leptons. This fact is usually stated as lepton number (L) being conserved. Consider the interactions given in Eq. 19. In the expression for neutron decay, the neutron and proton are baryons with $L = 0$. The beta particle has $L = 1$ and the anti-neutrino has $L = -1$. Before and after the decay, the total number of leptons is 0 and therefore L is conserved. This is also similar for the inverse beta decay reaction, where $L = 1$ before and after the interaction.

$$\begin{aligned} n &\rightarrow p + \beta^- + \bar{\nu}_e \\ \nu_e + n &\rightarrow p + \beta^- \end{aligned} \quad (19)$$

Terms such as $(\bar{\nu}_L)^c \nu_L$ in Eq. 18 result in interactions that change L by 2 units. That is, L would not be conserved. Therefore, due to such an interaction, the $\bar{\nu}_e$ produced in beta decay could initiate the inverse beta decay reaction with the result that $\Delta L = 2$. In fact, this pair of processes was actually one of the early proposed tests of Majorana neutrinos (Pontecorvo, 1957, 1958).

One important feature of the seesaw mechanism is the prediction of not only light, but also heavy Majorana neutrinos. There are numerous searches for both such particles through the $\Delta L = 2$ processes they would mediate. Figure 2 displays a generic $\Delta L = 2$ process involving an exchanged Majorana neutrino.

D. Leptogenesis

The seesaw model described above, not only gives insight into the smallness of ν mass, it also provides a mechanism to explain the matter-antimatter asymmetry of the Universe. This mechanism is called leptogenesis (Fukugita and Yanagida, 1986) and recent reviews are available (Buchmüller *et al.*, 2005; Davidson *et al.*, 2008; Di Bari, 2012).

The general requirements for a dynamical process to produce this asymmetry were identified in 1967 by A. Sakharov (Sakharov, 1967). First, the conservation of baryon number (B), the number of protons and neutrons, must be violated in some process. Second, charge-conjugation and space-inversion (CP) conservation must also be violated. If CP is conserved, then the rate of a

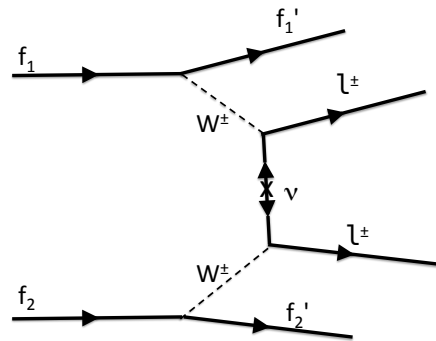


FIG. 2 Generic diagram showing a $\Delta L = 2$ process involving the exchange of a Majorana neutrino. f is a generic fermion, W^\pm is the weak interaction intermediate vector boson, and l^\pm is an outgoing lepton. The two W and l have the same charge for this $\Delta L = 2$ process.

process will be identical to the related process where all particle charges are reversed (i.e. $Q \rightarrow -Q$) and spatial coordinates are inverted (i.e. $\mathbf{r} \rightarrow -\mathbf{r}$). Finally, the processes that violate these conservation laws must take place out of equilibrium.

The Big Bang would have produced the heavy neutrinos, ν_{RS} with large mass m_R . The decay of these ν_{RS} into leptons and Higgs ($h^{0,\pm}$) may be written:

$$\nu_R^k \rightarrow l_j^+ + h^- \quad (20)$$

$$\nu_R^k \rightarrow l_j^- + h^+ \quad (21)$$

and

$$\nu_R^k \rightarrow \nu_j + h^0 \quad (22)$$

$$\nu_R^k \rightarrow \bar{\nu}_j + \bar{h}^0, \quad (23)$$

where the indices k and j run over lepton flavor ($l_j \in e, \mu, \tau$) and the two equation groupings are each for a pair of CP-transformed processes. The rates of each process within a pair may not be equal if CP conservation is violated. As the temperature of the Universe fell below a value near that of m_R , the decay and production of ν_R fell out of equilibrium because the production becomes energetically discouraged. As a result of this CP conservation violation and non-equilibrium, unequal numbers of leptons and anti-leptons would have arisen. This net lepton number (L) would have been converted to a net baryon number through standard model processes. This leptogenesis process therefore possesses all of the Sakharov requirements. It is presently an active area of research into the origin of the matter, anti-matter asymmetry.

For the purposes of this article, this is a minimal view of leptogenesis, but even for more sophisticated versions, there are two neutrino characteristics that must be established. First, neutrinos must be Majorana particles,

which is a natural consequence of the seesaw mechanism. Second, there must be CP violation in the lepton sector. Both of these are intense areas of experimental effort. If neutrinos are shown to be Majorana, it will be yet another clue as to our origins.

E. Double Beta Decay

The search for double beta decay ($\beta\beta$) is primarily motivated by its ability to demonstrate that neutrinos are Majorana, if that happens to be the case. It is a second order, weak process closely related to beta decay. Most nuclei that have both an even number of protons and neutrons are stable against beta decay. That is, the process

$${}^N_Z A \rightarrow {}^{N-1}_{Z+1} A + \beta^- + \bar{\nu}_e, \quad (24)$$

is energetically forbidden in most nuclei of mass number A that have an even atomic number Z and even neutron number N . In even-even nuclei for which beta decay is allowed, the rate is greatly inhibited. For a large number of even-even nuclei, however, the second order process with Z changing by 2 units, while emitting 2 electrons and 2 anti-neutrinos is allowed:

$${}^N_Z A \rightarrow {}^{N-2}_{Z+2} A + 2\beta^- + 2\bar{\nu}_e. \quad (25)$$

This process is called two-neutrino double beta decay ($\beta\beta(2\nu)$). As the 2 β^- s are leptons and the 2 $\bar{\nu}_e$ s are anti-leptons, the total lepton number before and after the decay is unchanged and L is conserved. $\beta\beta(2\nu)$ is expected within the standard model and has been observed in about 10 isotopes (Barabash, 2010).

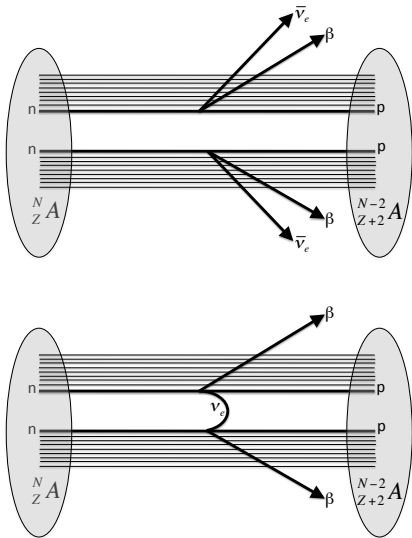


FIG. 3 Diagrams showing the $\beta\beta(2\nu)$ (top) and $\beta\beta(0\nu)$ (bottom) processes. Within the group of nucleons inside a nucleus, two neutrons simultaneously emit β particles while producing protons.

An alternative process that emits no neutrinos is written

$${}^N_Z A \rightarrow {}^{N-2}_{Z+2} A + 2\beta^-. \quad (26)$$

This zero-neutrino, or neutrinoless double beta decay ($\beta\beta(0\nu)$) process violates lepton number by 2 units. Diagrams representing $\beta\beta(2\nu)$ and $\beta\beta(0\nu)$ are shown in Fig. 3. Note the common features of the $\beta\beta(0\nu)$ panel in this figure to that of Fig. 2.

In experiments designed to directly detect $\beta\beta$, the two decay modes are distinguished by the energy carried off by the exiting β particles. (Section IV.A.1 discusses the various experimental issues.) The spectra are shown in Fig. 4. Since the neutrinos interact too weakly for their energy to be feasibly observed, the $\beta\beta(2\nu)$ spectrum of the sum of the electron energies is a continuum up to the total available energy for the decay. In contrast, the sum of the energies of the two electrons in $\beta\beta(0\nu)$ is a mono-energetic peak at that endpoint.

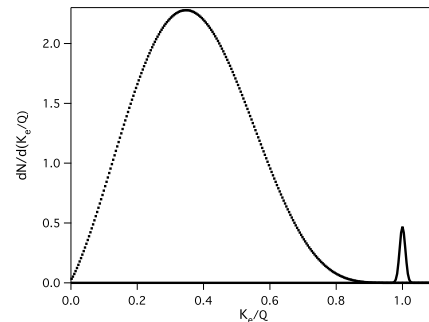


FIG. 4 The spectrum of the sum of the energies of the two electrons from $\beta\beta(2\nu)$ (dotted) and $\beta\beta(0\nu)$ (solid). The resolution used for $\beta\beta(0\nu)$ is arbitrary and the relative strength of $\beta\beta(0\nu)$ to that of $\beta\beta(2\nu)$ is exaggerated for clarity. In reality, if $\beta\beta(0\nu)$ exists, the peak would be very weak.

It may seem ironic that one can learn about neutrinos from a process that produces no neutrinos. The key to understanding this apparent non sequitor lies in Fig. 3. In the standard model, when a neutron decays it emits an $\bar{\nu}_e$, whereas a neutron can only absorb a ν_e . If the neutrino and anti-neutrino are distinct particles, the exchange depicted in the lower panel of that figure cannot occur. If the exchange does take place, there is no such distinction and neutrinos must be Majorana particles.

Figure 3 depicts $\beta\beta(0\nu)$ proceeding through the exchange of a light mass neutrino. It is known that neutrinos have a small mass (Fogli *et al.*, 2012), although the magnitude of that mass is not yet known. Since we know light neutrinos exist, this light-neutrino exchange is the most commonly considered mechanism for $\beta\beta(0\nu)$ in the literature. Numerous other possibilities have been proposed over the years. (See Ref. (Gehman and Elliott, 2007) and references therein for a list.) It should, however, be mentioned that if some other mechanism does

mediate the decay, an observation of $\beta\beta(0\nu)$ still implies that neutrinos are massive Majorana particles (Schechter and Valle, 1982).

The decay rate for $\beta\beta(0\nu)$ can be written:

$$[T_{1/2}^{0\nu}]^{-1} = G^{0\nu} |M_{0\nu}|^2 \langle m_{\beta\beta} \rangle^2 \quad (27)$$

where $T_{1/2}^{0\nu}$ is the half-life of the decay, $G^{0\nu}$ is the kinematic phase space factor, $M_{0\nu}$ is the matrix element corresponding to the $\beta\beta(0\nu)$ transition, and $\langle m_{\beta\beta} \rangle$ is the effective Majorana neutrino mass. $G^{0\nu}$ contains the kinematic information about the final state particles, and is calculable to the precision of the input parameters. $M_{0\nu}$ is difficult to calculate with an accuracy estimated to be approximately a factor of 2. One immediately notices from Eq. 27 that the decay rate is directly related to the Majorana neutrino mass. As the neutrino mass trends toward zero, the decay rate will also. In general, as the neutrino mass vanishes, it becomes impossible to discern the Dirac or Majorana nature of the neutrino.

The weak eigenstates of neutrinos, the quantum states produced during a weak interaction such as β decay, are not identical to the mass eigenstates. As a consequence, neutrinos will *oscillate* between the weak eigenstates as they propagate through space. This empirical fact has permitted the use of interferometry to study many neutrino characteristics including the difference between the mass eigenvalues and the mixing matrix elements that describe the oscillations. (A review of neutrino oscillations can be found in Ref. (Balantekin and Haxton, 2013).) The value of $\langle m_{\beta\beta} \rangle$ depends on these mixing angles and mass eigenvalues. If the neutrino is Majorana, then one can derive an expression for $\langle m_{\beta\beta} \rangle$ that includes data from neutrino oscillation experiments. It is written

$$\begin{aligned} \langle m_{\beta\beta} \rangle^2 &= \left| \sum_{i=1}^3 U_{ei}^2 m_i \right| \\ &= |U_{e1}^2 m_1 + U_{e2}^2 m_2 + U_{e3}^2 m_3| \\ &= |m_1 c_{12}^2 c_{13}^2 + m_2 s_{12}^2 c_{13}^2 e^{i\alpha_{21}} + m_3 s_{13}^2 e^{i\alpha_{31}}|. \end{aligned} \quad (28)$$

where m_i are the mass eigenvalues and the U_{ei} are the mixing matrix elements. The final line of Eq. 28 expresses the mixing matrix element in terms of mixing angles with the notation $c_{12} \equiv \cos\theta_{12}$. There are two phases that appear (α_{21}, α_{31}) that arise because of the Majorana nature of the neutrino.

Neutrino oscillation experiments are insensitive to the Majorana-Dirac nature of the neutrino. Importantly, these experiments also cannot determine the absolute mass scale of the neutrino. Such experiments only determine mass differences and hence a relationship between the three m_i . (To be technically correct, these experiments determine the differences in the masses squared.) As a result, the oscillation experiments have some, but not perfect, predictive power for the value of $\langle m_{\beta\beta} \rangle$, and therefore $T_{1/2}^{0\nu}$, if neutrinos are Majorana particles. There is a region of $\langle m_{\beta\beta} \rangle$ between about 15 and 50 meV, where

an optimist would expect to see $\beta\beta(0\nu)$. This region is referred to as the inverted-hierarchy or atmospheric mass region. It originates if the dominate contributions to $\langle m_{\beta\beta} \rangle$ arise from the heavier mass values associated with oscillation channels first observed in atmospheric neutrinos. A more pessimistic view is that $\langle m_{\beta\beta} \rangle$ would be a few meV or less, the so-called normal-hierarchy or solar mass region. This mass region arises from the lighter mass values associated with oscillation results first observed in solar neutrinos.

If one makes a plot of $\langle m_{\beta\beta} \rangle$ versus the lightest neutrino mass (Fig. 5) using what is known about the angles and mass differences, the result will be a band, as opposed to a line, due to the unknown phases. One will also see that two bands appear in such a figure, one for the normal and one for the inverted hierarchy that blend as one approaches a regime where all three mass eigenvalues are roughly equal, the degenerate region.

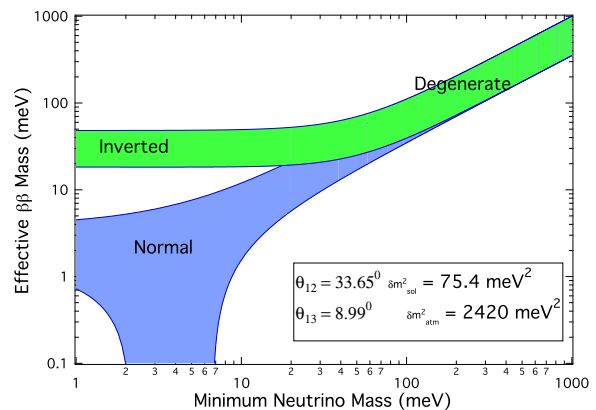


FIG. 5 $\langle m_{\beta\beta} \rangle$ as a function of the smallest of the three mass eigenvalues. The plot is done for the best fit oscillation parameters (Fogli *et al.*, 2012).

For the inverted hierarchy region, $T_{1/2}^{0\nu}$ is expected to be about 10^{27} y. From Eq. 27, it is clear that if $\langle m_{\beta\beta} \rangle$ is a factor of 10 less, that is within the normal hierarchy region, then $T_{1/2}^{0\nu}$ would be near 10^{29} y. The next generation of experiments (Sec. IV.A.1) are aiming to explore the inverted hierarchy region, with longer term R&D aimed at exploring the normal hierarchy region if nothing is observed at the shorter half-life.

F. Supersymmetry

The Standard Model (SM) has been very successful describing observed phenomena up to an energy scale of about a TeV. Even so, there are a number of deficiencies. These include the existence of dark matter, neutrino masses, the matter-antimatter asymmetry, and why the interaction strength of the known forces varies so greatly (the hierarchy problem).

Supersymmetry (Aitchison, 2009) (SUSY) is a proposed extension to the SM that would address these

shortcomings. SUSY relates bosons to fermions through a new symmetry that joins a fermion (boson) into a supermultiplet with a boson (fermion). When all the known particles are placed into supermultiplets, one finds that no known particles are available to fill the role of the superpartners. That is, half the particles required by SUSY have yet to be observed.

Particles within such a supermultiplet share properties, although they have differing spins. The supermultiplet that contains the spin 1 photon will contain a new spin $\frac{1}{2}$ particle, referred to as the photino. Since the photon is its own antiparticle, so would be the photino. Since the photino is spin $\frac{1}{2}$, if it exists, it would be a Majorana particle. In practice, there are 3 such new particles (photino, Zino, Higgsino) that would mix and the combination is called the neutralino. If this neutralino was the lightest supersymmetric particle (LSP), it would be long-lived and might be the dark matter. Although other SUSY LSP candidates that are not Majorana in nature might also be dark matter candidates, SUSY provides for some Majorana dark matter candidates.

In general, SUSY predicts the existence of Majorana particles. The search for such particles is described in Sections IV.A.2 and IV.A.4.

III. MAJORANA FERMIONS IN SOLID STATE DEVICES

Majorana fermions have been of great interest in condensed matter physics over the past decade. In this review we shall focus on solid state systems in which Majorana fermions arise as emergent quasiparticles of the underlying superconducting state. Although there are other proposed realizations, superconducting systems are conceptually simplest, best understood, and arguably closest to unambiguous physical realization and detection. There exist several excellent reviews of this topic aimed at the condensed matter audience (Alicia, 2012; Beenakker, 2013a; Stanescu and Tewari, 2013). By contrast, our objective here is to present the topic to a broader audience of physicists who possess basic understanding of condensed matter physics but are not specialists. Consequently, we shall focus on communicating the key ideas underlying the emergence of Majorana particles in solid-state devices. We illustrate these ideas on simple toy models and describe how these can be generalized to apply in more realistic physical systems. Finally, in Sec. V we discuss recent attempts to engineer and detect Majorana fermions experimentally. Readers who desire a more advanced and complete discussion are referred to the above mentioned review articles and the original literature.

A. Majorana fermions as emergent particles in topological superconductors

1. General considerations

To set the stage we first briefly review the Bogoliubov-de Gennes (BdG) formalism that is used to describe solids with superconducting order. This is, in essence, the venerable BCS theory of superconductivity (Bardeen *et al.*, 1957), adapted to describe spatially non-uniform situations. We use this formalism to elucidate how Majorana fermions can arise in superconductors on general grounds. In later subsections we then give specific examples of this general principle and connect these examples to the ongoing experimental studies.

Superconductivity arises when electrons in a metal experience attractive interaction. In ordinary superconductors this attraction is known to originate from the electron-phonon coupling but other mechanisms have been proposed to operate in high- T_c cuprate and other unconventional superconductors. For our purposes the origin of the attraction will be unimportant and we describe the superconductor by the following minimal model,

$$\mathcal{H} = \int d^d r \left[h_0^{\sigma\sigma'}(\mathbf{r}) c_{\sigma\mathbf{r}}^\dagger c_{\sigma'\mathbf{r}} - V n_{\uparrow\mathbf{r}} n_{\downarrow\mathbf{r}} \right]. \quad (29)$$

Here $c_{\sigma\mathbf{r}}^\dagger$ creates an electron with spin σ at the spatial point \mathbf{r} , $n_{\sigma\mathbf{r}} = c_{\sigma\mathbf{r}}^\dagger c_{\sigma\mathbf{r}}$ represents the number operator. The first term in Eq. (29) describes the kinetic energy of the electrons and any single-electron potential while the second term represents the attractive interaction with $V > 0$. In the simplest case of free electrons $h_0^{\sigma\sigma'}(\mathbf{r}) = (\hbar^2 \nabla^2 / 2m - \mu) \delta_{\sigma\sigma'}$ but we shall see that a more complicated form of the kinetic energy that includes spin-orbit coupling (or alternately more complicated interaction term) is required to achieve topological phase.

To proceed we now perform the Bogoliubov mean-field decoupling of the interaction term, writing

$$\begin{aligned} -n_{\uparrow\downarrow} &= c_{\uparrow\downarrow}^\dagger c_{\downarrow\uparrow} c_{\uparrow\downarrow} \\ &\simeq \langle c_{\uparrow\downarrow}^\dagger c_{\downarrow\uparrow} \rangle c_{\uparrow\downarrow} + c_{\uparrow\downarrow}^\dagger \langle c_{\downarrow\uparrow} c_{\uparrow\downarrow} \rangle - \langle c_{\uparrow\downarrow}^\dagger c_{\downarrow\uparrow} \rangle \langle c_{\uparrow\downarrow} c_{\uparrow\downarrow} \rangle, \end{aligned} \quad (30)$$

where the expectation values are taken with respect to the mean-field Hamiltonian specified below and we have suppressed the spatial index for brevity. If we now define the SC order parameter

$$\Delta(\mathbf{r}) = V \langle c_{\uparrow\mathbf{r}} c_{\downarrow\mathbf{r}} \rangle, \quad (31)$$

we can write down the BdG mean-field Hamiltonian

$$\begin{aligned} \mathcal{H}_{\text{MF}} &= \int d^d r \left[h_0^{\sigma\sigma'}(\mathbf{r}) c_{\sigma\mathbf{r}}^\dagger c_{\sigma'\mathbf{r}} \right. \\ &\quad \left. + \left(\Delta(\mathbf{r}) c_{\uparrow\mathbf{r}}^\dagger c_{\downarrow\mathbf{r}}^\dagger + \text{h.c.} \right) - \frac{1}{V} |\Delta(\mathbf{r})|^2 \right]. \end{aligned} \quad (32)$$

As the final step we define a four-component Nambu spinor

$$\hat{\Psi}_{\mathbf{r}} = \begin{pmatrix} c_{\uparrow\mathbf{r}} \\ c_{\downarrow\mathbf{r}} \\ -c_{\downarrow\mathbf{r}}^\dagger \\ c_{\uparrow\mathbf{r}}^\dagger \end{pmatrix} \equiv \begin{pmatrix} \hat{\psi}_{\mathbf{r}} \\ i\sigma^y \hat{\psi}_{\mathbf{r}}^* \end{pmatrix}, \quad (33)$$

where the hat symbol reminds us that $\hat{\Psi}_{\mathbf{r}}$ is an operator. This allows the BdG Hamiltonian to be cast into a compact form

$$\mathcal{H}_{\text{MF}} = \int d^d r \left[\hat{\Psi}_{\mathbf{r}}^\dagger H_{\text{BdG}}(\mathbf{r}) \hat{\Psi}_{\mathbf{r}} - \frac{1}{V} |\Delta(\mathbf{r})|^2 \right], \quad (34)$$

with

$$H_{\text{BdG}}(\mathbf{r}) = \begin{pmatrix} h_0(\mathbf{r}) & \Delta(\mathbf{r}) \\ \Delta^*(\mathbf{r}) & -\sigma^y h_0^*(\mathbf{r}) \sigma^y \end{pmatrix}. \quad (35)$$

In the last equation h_0 and Δ should be viewed as 2×2 matrices in spin space while $\boldsymbol{\sigma} = (\sigma^x, \sigma^y, \sigma^z)$ denotes the corresponding vector of Pauli matrices. It is useful at this point to introduce another set of Pauli matrices $\boldsymbol{\tau} = (\tau^x, \tau^y, \tau^z)$ acting in the Nambu space, i.e. the 2×2 matrix structure explicitly displayed in Eq. (35). It is also useful to remark that the lower diagonal block of H_{BdG} is the time-reversed version of $h_0(\mathbf{r})$, the time-reversal operator for spin- $\frac{1}{2}$ fermions being of the form $\Theta = i\sigma^y K$ with K denoting the complex conjugation.

The problem specified by the Hamiltonian (34) and the self-consistency condition (31) can now be solved by seeking a set of eigenfunctions $\Phi_n(\mathbf{r}) = [u_{n\uparrow}(\mathbf{r}), u_{n\downarrow}(\mathbf{r}), v_{n\uparrow}(\mathbf{r}), v_{n\downarrow}(\mathbf{r})]^T$ and eigenvalues E_n satisfying

$$H_{\text{BdG}}(\mathbf{r}) \Phi_n(\mathbf{r}) = E_n \Phi_n(\mathbf{r}). \quad (36)$$

In the basis spanned by these eigenfunctions the Hamiltonian (34) is brought to a diagonal form,

$$\mathcal{H}_{\text{MF}} = \sum_n E_n \hat{\psi}_n^\dagger \hat{\psi}_n + E_g \quad (37)$$

where E_g is a constant representing the ground-state energy and

$$\hat{\psi}_n = \int d^d r \Phi_n^\dagger(\mathbf{r}) \hat{\Psi}_{\mathbf{r}} \quad (38)$$

is an eigenmode operator that annihilates the Bogoliubov quasiparticle with energy E_n . The full solution to the problem now can be obtained by expressing $\Delta(\mathbf{r})$ in Eq. (31) through the eigenfunctions $\Phi_n(\mathbf{r})$ and iterating the resulting gap equation along with Eq. (36) until self-consistency is achieved. It is worth mentioning that for an infinite uniform system the ground state of \mathcal{H}_{MF} coincides with the famed BCS wavefunction which is in turn known to represent an exact ground state of the interacting Hamiltonian (29). For spatially non-uniform

systems and at non-zero temperature T the BdG formalism is widely believed to provide an exceedingly accurate description of the system. Before we move on we take this opportunity to remind the reader of one important generic feature of superconductors that follows directly from the above treatment. In the spatially uniform situation with $\Delta(\mathbf{r}) = \Delta_0$ and when h_0 is diagonal in spin indices, the spectrum of excitations can be easily found by passing to the momentum representation and reads

$$E_{\mathbf{k}} = \sqrt{(\epsilon_{\mathbf{k}} - \mu)^2 + \Delta_0^2}. \quad (39)$$

Here $\epsilon_{\mathbf{k}}$ is the normal-state electron dispersion and Eq. (39) implies a gap of the size $|\Delta_0|$ in the excitation spectrum.

In the development leading to Eq. (37) we glossed over an important subtlety that will prove crucial for our understanding of the origin of Majorana fermions in superconducting systems. It is easy to check that when passing from Eq. (32) to (34) we have inadvertently *doubled* the number of degrees of freedom in order to accommodate the pairing term. This is easiest to see by inspecting the BdG Hamiltonian (35) which is represented by a matrix twice the size of the normal-state Hamiltonian $h_0(\mathbf{r})$. This is the well-known phenomenon of BdG ‘doubling’. Another way to ascertain this is to note that only two components of the spinor $\hat{\Psi}_{\mathbf{r}}$ defined in Eq. (33) are independent; the lower two components are related to the upper two by Hermitian conjugation. Indeed it holds

$$C \hat{\Psi}_{\mathbf{r}}^* = \hat{\Psi}_{\mathbf{r}}, \quad (40)$$

where $\hat{\Psi}_{\mathbf{r}}^* = (\hat{\Psi}_{\mathbf{r}}^\dagger)^T$ and

$$C = \tau^y \sigma^y = \begin{pmatrix} 0 & -i\sigma^y \\ i\sigma^y & 0 \end{pmatrix} \quad (41)$$

is the charge conjugation matrix.

The redundancy inherent to the BdG description is resolved by observing that $H_{\text{BdG}}(\mathbf{r})$ has a particle-hole (charge conjugation) symmetry expressed as

$$C H_{\text{BdG}}^*(\mathbf{r}) C^\dagger = -H_{\text{BdG}}(\mathbf{r}), \quad (42)$$

which implies that for each eigenstate $\Phi_n(\mathbf{r})$ at energy E_n there exists an eigenstate $\Phi_n'(\mathbf{r}) = C \Phi_n^*(\mathbf{r})$ at energy $-E_n$. Thus the BdG redundancy can be eliminated by taking as physical only one of each pair of particle-hole conjugate eigenstates. Conventionally, one takes the eigenstates corresponding to the positive energy eigenvalues, in which case the eigenmode operators $\hat{\psi}_n^\dagger$ have the natural interpretation as creation operators of the positive-energy Bogoliubov excitations above the SC ground state. This can be seen directly from the structure of the Hamiltonian (37).

Alternately, the particle-hole symmetry noted in Eq. (42) can be viewed as a reality constraint on the BdG Hamiltonian. To see this more clearly one can perform a unitary transformation $H_{\text{BdG}} \mapsto \tilde{H}_{\text{BdG}} = U H_{\text{BdG}} U^\dagger$.

With $U = \frac{1}{2}(1 - \tau^y + \sigma^y + \tau^y\sigma^y)$ the condition (42) becomes simply

$$\tilde{H}_{\text{BdG}}^*(\mathbf{r}) = -\tilde{H}_{\text{BdG}}(\mathbf{r}), \quad (43)$$

informing us that $\tilde{H}_{\text{BdG}}(\mathbf{r})$ is purely imaginary. The corresponding time-dependent Schrödinger equation

$$-i\hbar\partial_t\tilde{\Phi}(\mathbf{r},t) = \tilde{H}_{\text{BdG}}(\mathbf{r})\tilde{\Phi}(\mathbf{r},t) \quad (44)$$

is then purely real and admits real solutions for the wavefunction $\tilde{\Phi}(\mathbf{r},t)$. If the normal state Hamiltonian h_0 is linear in spatial derivatives (as it is the case e.g. for a superconducting state induced on the surface of a topological insulator discussed below) then Eq. (44) becomes identical to the Dirac equation in the Majorana representation discussed in Sec. II. For a more general structure of h_0 Eq. (44) remains real, its solutions can be taken as purely real and can be thus viewed as describing Majorana fermions in a more general sense.

It is easy to see that in this basis the charge conjugation matrix $\tilde{C} = \mathbb{1}$. Therefore, Eq. (40) becomes simply $\hat{\Psi}_{\mathbf{r}}^* = \hat{\Psi}_{\mathbf{r}}$, informing us directly that the quantum field $\hat{\Psi}_{\mathbf{r}}$ pertains to a Majorana fermion. One can thus say that in the Majorana representation of the BdG theory defined by the Hamiltonian $\tilde{H}_{\text{BdG}}(\mathbf{r})$ the excitations of a superconductor possess the key attributes of Majorana fermions: they are electrically neutral fermions with no distinction between particles and antiparticles. This point of view has been generally appreciated for a long time but was carefully analyzed and formulated only recently (Chamon *et al.*, 2010).

Another similarity with particle physics follows from anomalous terms $c_{\uparrow\mathbf{r}}^\dagger c_{\downarrow\mathbf{r}}^\dagger$ appearing in the BdG Hamiltonian (32). These indicate events in which the number of electrons changes by $\Delta L = 2$, analogous to the lepton number non-conservation discussed in Sec. IIC. In the superconductor, the total number of electrons is of course strictly conserved, as one can see by inspecting the full interacting Hamiltonian (29) which commutes with the number operator. In the BdG description the number non-conservation reflects the fact that a pair of electrons can disappear (or emerge from) the superconducting condensate which is treated at the mean-field level. Such processes are real and have experimentally observable consequences (Beenakker, 2013b).

It may be concluded from the analysis presented above that Majorana fermions naturally appear in the theoretical description of a generic superconductor. Since the BCS theory and the related BdG formalism on which this description rests are in an excellent agreement with the large body of experimental data on superconductors it could be inferred that Majorana fermions are already well established in this context. In superconductors, the order parameter amplitude (i.e. the SC gap) plays the role of the Majorana mass and electron number non-conservation follows from the existence of the condensate. On the other hand physical properties of most superconductors can be understood perfectly well without

directly invoking Majorana's seminal work. The issue is also muddled by the fact that the Majorana character of the superconducting quasiparticles follows from the formal step of doubling the number of degrees of freedom in the BCS-BdG description. For these reasons the fundamental connection between the theory of superconductivity and the Majorana fermion concept in high-energy physics has not been fully appreciated until quite recently. There are however situations arising in the context of the so called *topological superconductors*, where it is instrumental to recognize the connection with Majorana's work. This is when isolated, unpaired Majorana fermions occur in a superconductor, typically as the zero modes of BdG Hamiltonian discussed below.⁴ In the rest of this Chapter we will focus on precisely such cases. These have been subject of intense theoretical and experimental studies over the past decade and remain among the most active subfields of condensed matter physics.

2. Majorana zero modes

A situation of particular interest arises when the spectrum of excitations in a superconductor is such that there exists a single mode with exactly zero energy,

$$H_{\text{BdG}}(\mathbf{r})\Phi_0(\mathbf{r}) = 0, \quad (45)$$

separated from all other modes by an energy gap. According to the discussion above we must conclude that, remarkably, only one half of that mode is actually physical. In addition, such a zero mode is self-conjugate under the symmetry defined in Eq. (42) meaning that

$$\Phi_0(\mathbf{r}) = \tau^y\sigma^y\Phi_0^*(\mathbf{r}), \quad (46)$$

or, written in terms of the individual components,

$$\begin{pmatrix} u_{0\uparrow} \\ u_{0\downarrow} \\ v_{0\uparrow} \\ v_{0\downarrow} \end{pmatrix} = \begin{pmatrix} -v_{0\downarrow}^* \\ v_{0\uparrow}^* \\ u_{0\downarrow}^* \\ -u_{0\uparrow}^* \end{pmatrix}, \quad (47)$$

where we have dropped the position argument for the sake of clarity. The zero-mode annihilation operator is now given by Eq. (38) which, when expanded, reads

$$\begin{aligned} \hat{\psi}_0 = i \int d^d r \Big[& u_{0\uparrow}^*(\mathbf{r})c_{\mathbf{r}\uparrow} + u_{0\downarrow}^*(\mathbf{r})c_{\mathbf{r}\downarrow} \\ & - v_{0\uparrow}^*(\mathbf{r})c_{\mathbf{r}\downarrow}^\dagger + v_{0\downarrow}^*(\mathbf{r})c_{\mathbf{r}\uparrow}^\dagger \Big], \end{aligned} \quad (48)$$

⁴ We will see later in this Section that such Majorana zero modes in fact do not obey fermionic exchange statistics but are so called “non-Abelian anyons”. For simplicity and in keeping with the current literature we will continue referring to these objects as “Majorana fermions” although it should be kept in mind that, strictly speaking, this is a misnomer.

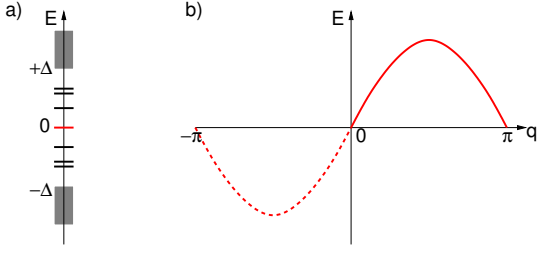


FIG. 6 a) Schematic energy excitation spectrum of a superconductor. Except for a possible zero-mode eigenstates come in pairs with opposite energy. b) The energy spectrum associated with a chain composed of Majorana fermions Eq. (53). Only half of the states in the Brillouin zone are physical, the remaining states are located at the opposite edge of the system.

where the arbitrary i factor has been added for convenience. With help of Eq. (47) it is now straightforward to verify that

$$\hat{\psi}_0^\dagger = \hat{\psi}_0, \quad (49)$$

informing us that the zero mode is a Majorana fermion.

The all-important distinction between such Majorana zero mode and a generic excitation in a superconductor is the following. A generic excitation is typically delocalized throughout the volume of the sample, or if localized it appears in a degenerate doublet with another such excitation. Thus although a formal description as a Majorana fermion is possible one can as well describe the pair of such Majoranas as an ordinary Dirac fermion. By contrast the zero mode is by construction non-degenerate and its description as a Majorana particle is therefore mandatory. In addition, when the zero mode is spatially localized, it then becomes possible to probe it experimentally. Such studies can be used to reveal the physical properties of an isolated Majorana fermion.

Several remarks are now in order:

- The discussion above makes it clear that if a Majorana zero mode exists in a system then it is topologically protected, provided that there is an energy gap (often called a ‘minigap’) separating it from all other states. The reason is that the zero mode cannot acquire a non-zero energy E_0 by any continuous deformation of the Hamiltonian that does not close the minigap. If this were so then the symmetry defined in Eq. (42) would require another mode to appear at energy $-E_0$. Appearance of a new mode would represent a discontinuity in the spectral evolution and this is not allowed under the constraints specified above. The situation is illustrated in Fig. 6a.
- A single unpaired Majorana zero mode can exist only in an infinite system. In systems of finite size Majorana modes always appear in pairs, reflecting

the fact that such systems always contain an integral number of electrons. Nevertheless, a situation of interest arises when the two Majorana zero modes are spatially separated so that their individual wavefunctions have a negligible overlap. In this case, when probed locally, the system exhibits unpaired Majorana zero modes. Also, in this situation Majorana modes can be moved away from zero energy without closing the minigap by simply bringing them close together so that the wavefunctions overlap. The two zero modes thus evolve into a pair of levels $(E_0, -E_0)$ with a splitting proportional to the overlap.

- A necessary condition to obtain unpaired Majorana zero modes in a system comprised of electrons is that the Hamiltonian breaks the time-reversal symmetry. This is because time-reversal invariance for spin- $\frac{1}{2}$ fermions implies Kramers degeneracy: for each state described by an eigenfunction $\Phi(\mathbf{r})$ there exists a distinct eigenstate, at the same energy, with wavefunction $\Theta\Phi(\mathbf{r})$, where Θ is an antiunitary operator implementing the time-reversal operation. Thus, in a \mathcal{T} -invariant electron system, Majorana zero modes always come in pairs located at the same spatial position.
- If there are several Majorana zero modes in the system it is easy to show that their associated annihilation operators $\hat{\psi}_{0j}$ formally satisfy the canonical commutation relations (11) characteristic of Majorana fermions. Upon closer examination, however, it turns out that their exchange statistics is more complicated and the zero modes should be correctly described as non-Abelian anyons. This very interesting property arises because of the extra contribution to the exchange statistics coming from the superconducting condensate and we will discuss it in more detail later in this Section. Non-Abelian exchange statistics also underlies the potential significance of Majorana zero modes for topological quantum computation.

Unpaired Majorana zero modes discussed thus far are localized objects that are typically associated with point-like defects present in topological superconductors. We will explain in the following subsections how they arise at the ends of 1D SC wires, in the vortex cores of 2D topological superconductors and other situations. We will also discuss their unusual properties that underlie much of the current interest in these exotic forms of quantum matter.

To illustrate the interesting properties of such Majorana zero modes we consider a simple example. Imagine we have at our disposal a 1D SC wire with Majorana zero modes at its ends. Now imagine an array of such wires arranged in parallel and weakly coupled so that the Majorana particles can hop between nearest neighbors. Denoting the Majorana mode on the j -th wire by γ_j the

simplest Hamiltonian describing such a system takes the form

$$\mathcal{H} = -it \sum_j \gamma_j \gamma_{j+1}, \quad (50)$$

where t is the tunneling amplitude and the factor i is necessary for the Hamiltonian to be hermitian. We now pass to the momentum space

$$\gamma_k = \frac{1}{\sqrt{N}} \sum_j e^{ikj} \gamma_j, \quad (51)$$

where N is the total number of sites and k extends over the first Brillouin zone $(-\pi, \pi)$. The Hamiltonian can be written as

$$\mathcal{H} = -it \sum_k e^{ik} \gamma_{-k} \gamma_k. \quad (52)$$

Since according to Eq. (51) the γ_k operators satisfy $\gamma_k^\dagger = \gamma_{-k}$ we can recast this into a more suggestive form

$$\mathcal{H} = -2t \sum_{k>0} \sin k \gamma_k^\dagger \gamma_k. \quad (53)$$

When restricted to one half of the Brillouin zone γ_k operators satisfy the algebra of ordinary fermionic particles analogous to Eqs. (9). This is easy to verify by combining Eqs. (51) and (12). The Hamiltonian (53) can thus be viewed as a describing ordinary Dirac fermions defined in one half of the Brillouin zone, as illustrated in Fig. 6b. It indicates that, as expected, the Hilbert space associated with a chain of Majorana fermions has half as many degrees of freedom as a chain formed by ordinary spinless fermions.

B. Kitaev chain: the 1D prototype system

The simplest model system that shows unpaired Majorana fermions is the Kitaev chain (Kitaev, 2001). It describes a 1D system of *spinless* fermions and for this reason it has been initially viewed as a somewhat unphysical toy model. However, it has been realized more recently that in the presence of spin-orbit coupling and the Zeeman field real electrons can in fact behave essentially like spinless fermions. Kitaev model, which is simple and exactly soluble, thus provides an extremely useful paradigm for Majorana fermions in one spatial dimension and for this reason we shall discuss it in some detail.

The Kitaev chain consists of spinless fermions hopping between the sites of a 1D lattice described by the Hamiltonian

$$\mathcal{H} = \sum_j \left[-t(c_j^\dagger c_{j+1} + \text{h.c.}) - \mu(c_j^\dagger c_j - \frac{1}{2}) + (\Delta c_j^\dagger c_{j+1}^\dagger + \text{h.c.}) \right], \quad (54)$$

where Δ represents the nearest-neighbor pairing amplitude, the simplest allowed possibility for SC order with spinless fermions. Henceforth we shall assume for the sake of simplicity that Δ is real and consider a chain with N sites and open boundary conditions. Using transformation (12) we can rewrite this Hamiltonian in the Majorana representation,

$$\mathcal{H} = \frac{i}{2} \sum_j \left[-\mu \gamma_{j1} \gamma_{j2} + (t + \Delta) \gamma_{j2} \gamma_{j+1,1} + (-t + \Delta) \gamma_{j1} \gamma_{j+1,2} \right]. \quad (55)$$

At this point it is useful to examine two specific limits. First, consider the case $\Delta = t = 0$. The Hamiltonian becomes simply

$$\mathcal{H} = \frac{i}{2} (-\mu) \sum_j \gamma_{j1} \gamma_{j2} = -\mu \sum_j (c_j^\dagger c_j - \frac{1}{2}). \quad (56)$$

The ground state consists of all fermion states at site j either occupied ($\mu > 0$) or empty ($\mu < 0$) and this is clearly a topologically trivial phase. Second, consider the case $\Delta = t$ and $\mu = 0$. Now the Hamiltonian takes the form

$$\mathcal{H} = it \sum_{j=1}^{N-1} \gamma_{j2} \gamma_{j+1,1}. \quad (57)$$

The ground state of this Hamiltonian is easily found by defining a new set of fermionic operators

$$a_j = \frac{1}{2}(\gamma_{j2} + i\gamma_{j+1,1}), \quad a_j^\dagger = \frac{1}{2}(\gamma_{j2} - i\gamma_{j+1,1}), \quad (58)$$

for $j = 1, 2, \dots, N-1$. These live on nearest neighbor bonds of our 1D chain as illustrated in Fig. 7b. In terms of these new fermions we have

$$\mathcal{H} = 2t \sum_{j=1}^{N-1} (a_j^\dagger a_j - \frac{1}{2}), \quad (59)$$

and the ground state for $t > 0$ is simply an a_j vacuum with total energy $E_g = -t(L-1)$. The remarkable thing is that Hamiltonian (57) does not contain operators $\gamma_{1,1}$ and $\gamma_{N,2}$. These represent zero-energy Majorana fermions localized at the ends of the chain. Together they encode one Dirac fermion which is fundamentally delocalized between the two ends of the chain. We remark that similar considerations yield unpaired Majorana fermions also for the special case $\Delta = -t$ and $\mu = 0$.

The two special cases considered above represent two distinct phases of the Kitaev model: the trivial phase and the topological phase with unpaired Majorana fermions localized at its ends. To show that these indeed correspond to stable phases consider the same Hamiltonian (54) but now with periodic boundary conditions. In momentum space it can be written as

$$\mathcal{H} = \sum_q \left[(-2t \cos q - \mu) c_q^\dagger c_q + \Delta (i \sin q c_q c_{-q} + \text{h.c.}) \right], \quad (60)$$

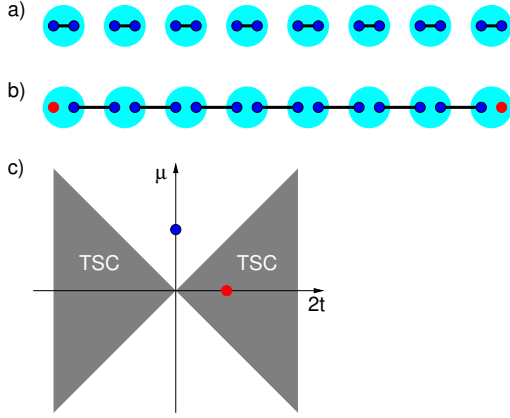


FIG. 7 Two phases of the Kitaev chain. a) In the trivial phase Majorana fermions on each lattice site can be thought of as bound into ordinary fermions. b) In the topological phase Majoranas on neighboring sites are bound leaving two unpaired Majorana fermions at the ends of the chain. c) The phase diagram of the Kitaev chain in the μ - $2t$ plane, showing the topological phase (TSC) and the normal phase. The blue and the red dot mark the special points in the parameter space considered in the text.

and has an excitation spectrum of the form

$$E(q) = \pm \sqrt{(2t \cos q + \mu)^2 + (\Delta \sin q)^2}. \quad (61)$$

If we now focus on the superconducting phases (i.e. $\Delta \neq 0$) then it is easy to see that the excitation spectrum Eq. (61) remains fully gapped except when $2t = \pm\mu$. This condition defines two lines, indicated in Fig. 7, which mark the phase boundaries between the two stable phases of the model. (We are making use of the general principle of adiabatic continuity which states that two gapped phases are identical if they can be smoothly deformed into one another without closing the excitation gap.) We identify the region $|2t| > |\mu|$ as the topological phase since the second special point considered above lies within this phase. The other phase is topologically trivial.

Since the two phases have the same physical symmetries the transition between them is a special type of a phase transition called topological phase transition. The two phases are distinguished by the presence or absence of unpaired Majorana fermions at the ends in the geometry with open boundary conditions. The question that naturally arises and that will have important consequences in our search for topological phases in realistic systems is the following. In the absence of symmetry distinction is it possible to distinguish the topological phase from the trivial phase by studying the bulk of the system? The answer is affirmative: such phases can be distinguished by means of *topological invariants*. Among the better known topological invariants are the Chern number, allowing one to differentiate between different quantum Hall phases in two-dimensional quantum

Hall systems, and the more recently discovered Z_2 invariants that characterize topological insulators in two and three dimensions. For 1D topological superconductors the relevant topological invariant is the Majorana number $\mathcal{M} = \pm 1$ first formulated by Kitaev (Kitaev, 2001). In his seminal 2001 paper Kitaev showed that all 1D fermionic systems with SC order fall into two categories distinguished by \mathcal{M} . Presence of unpaired Majorana fermions is indicated when $\mathcal{M} = -1$.

As topological invariants go \mathcal{M} is easy to evaluate (although the reasoning behind its formulation is more involved and we refer the interested reader to the original Kitaev paper). A Hamiltonian for any non-interacting translationally invariant fermionic system in 1D can be written in the Majorana representation as

$$\mathcal{H} = \frac{i}{4} \sum_{lm\alpha\beta} B_{\alpha\beta}(l-m) \gamma_{l\alpha} \gamma_{m\beta}, \quad (62)$$

where l, m denote the lattice sites while α, β label all other quantum numbers, including spin and orbital degrees of freedom. The Majorana number is defined as

$$\mathcal{M} = \text{sgn} \left\{ \text{Pf}[\tilde{B}(0)] \text{Pf}[\tilde{B}(\pi)] \right\}, \quad (63)$$

where $\tilde{B}(q)$ denotes the spatial Fourier transform of $B(l-m)$ viewed as a matrix in indices α, β and $\text{Pf}[A]$ denotes the Pfaffian. For $q = 0, \pi$ matrix $\tilde{B}(q)$ is anti-symmetric (this follows from the requirement that \mathcal{H} is hermitian) and the Pfaffian is thus well defined. For a known matrix of a small size the Pfaffian is readily evaluated. The topological invariant for a 1D superconductor can be therefore easily computed directly from the system's Hamiltonian. We will present a concrete example of such a computation below.

An important conceptual tool follows from studying the limit of weak SC order, i.e. the situation when Δ is much smaller than all relevant energy scales in the problem, such as the bandwidth, which is typically the case in most superconductors. In this limit one can show that Eq. (63) further simplifies to

$$\mathcal{M} = (-1)^\nu, \quad (64)$$

where ν represents the number of Fermi points q_F of the underlying normal system ($\Delta = 0$) in the interval $(0, \pi)$. This formulation provides a simple but extremely useful guide to searches for topological superconductors in 1D: one is compelled to look for 1D metals with an odd number of Fermi points in the right half of the Brillouin zone. Such 1D metals, when made superconducting, form a topological phase with unpaired Majorana fermions localized at their ends.

We close this subsection by evaluating \mathcal{M} for the Kitaev model using Eq. (63). To this end passing into momentum space as in Eq. (51) we can write the Kitaev Hamiltonian (55) in the following form,

$$\mathcal{H} = \frac{i}{4} \sum_q (\gamma_{q1}, \gamma_{q2}) \begin{pmatrix} 0 & D_q \\ -D_q^* & 0 \end{pmatrix} \begin{pmatrix} \gamma_{-q1} \\ \gamma_{-q2} \end{pmatrix}, \quad (65)$$

with $D_q = -\mu - 2t \cos q - 2i\Delta \sin q$. Pfaffian of a 2×2 antisymmetric matrix is simply given by its upper off-diagonal component which yields the Majorana number

$$\mathcal{M} = \text{sgn}(D_0 D_\pi) = \text{sgn}(\mu^2 - 4t^2). \quad (66)$$

The topological phase occurs when $\mathcal{M} = -1$, or $|\mu| < 2|t|$, in accord with our earlier analysis. One can also test Eq. (64). When $\Delta = 0$ the normal state dispersion of the Kitaev chain becomes $\epsilon(q) = -2t \cos q - \mu$. This yields one Fermi point between $(0, \pi)$ when $|\mu| < 2|t|$ and no Fermi points otherwise, confirming once again the structure of the topological phase diagram indicated in Fig. 7c.

C. Physical realizations in 1D

The key obstacle standing in the way of physical realizations of Kitaev's paradigm is the electron spin. In most natural realizations of a 1D chain, electron spin causes all bands to be doubly degenerate thus preventing the desirable situation with an odd number of Fermi points, required for the emergence of the topological phase according to the discussion in the previous subsection. Below we discuss special situations in which this problem can be avoided. They involve various combinations of the spin-orbit coupling and magnetic interactions that produce a normal metal that is effectively spinless. Superconductivity is then induced through the proximity effect, whereby pairing occurs due to Cooper pair tunneling from a nearby superconductor.

1. Edge of a 2D topological insulator

Topological insulators (TIs) are materials with gapped insulating bulk and topologically protected gapless surface states (Franz and Molenkamp, 2013; Hasan and Kane, 2010; Moore, 2010; Qi and Zhang, 2011). The surface states form an unconventional metal and are protected by time reversal symmetry \mathcal{T} . This remarkable behavior comes about as a result of strong spin-orbit coupling and occurs in crystals and alloys made of heavy non-magnetic elements. Canonical examples of TIs include HgTe quantum wells, $\text{Bi}_x\text{Sb}_{1-x}$ alloys and Bi_2Se_3 crystals.

The edge of a 2D TI is characterized by a pair of counter-propagating, spin filtered, linearly dispersing edge states, illustrated in Fig. 8b. The relevance of such an edge for the emergence of Majorana fermions stems from the fact that when the chemical potential resides inside the bulk bandgap the state can be viewed as a 1D system with an odd number of Fermi points in the right half of the Brillouin zone. Thus, according to the Kitaev criterion, one expects such an edge to form a foundation for a 1D topological superconductor if superconductivity can be induced, e.g. by the proximity effect. One important subtlety stems from the fact that being a boundary

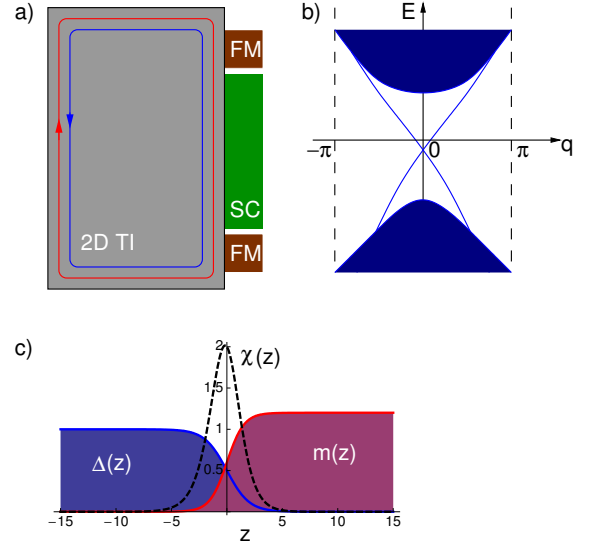


FIG. 8 a) 2D topological insulator interfaced with a superconductor (SC) and two ferromagnetic insulators (FM). Majorana Fermions are expected to occur at the SC/FM boundaries. b) Schematic spectrum of the surface state in a 2D TI. The shaded regions represent the bulk conduction and valence bands. c) SC and magnetic order parameter profiles near the SC/FM boundary assumed in the calculation. The dashed line shows the resulting Majorana wavefunction amplitude.

of a 2D system, the edge does not have an end. In order to localize the expected Majorana fermions one must employ a setup illustrated in Fig. 8a with a TI edge interfaced with a superconductor and a magnetic insulator (Fu and Kane, 2009). The magnetic material also provides the \mathcal{T} -breaking that is necessary to obtain unpaired Majorana fermions. As we shall show momentarily, Majorana fermions arise at the boundary between the SC and magnetic regions of the edge.

The low-energy theory of the edge modes is described by the Bloch Hamiltonian

$$h_0(q) = vq\sigma^y + m\sigma^x - \mu \quad (67)$$

where v is the mode velocity and m represents the x -component of the magnetic order induced by the proximate magnetic insulator. We are selecting specific quantization directions in the spin space but the only important feature is that the magnetic order has a component perpendicular to the electron spin. In this case the spectrum of excitations reads $\epsilon(q) = \pm\sqrt{v^2q^2 + m^2} - \mu$ and is illustrated in Fig. 8b. Magnetic order will gap out the surface mode if $|\mu| < |m|$. This explains why magnetic order can be thought of as effectively ending the wire. Since we shall be interested in spatially varying situations we now pass into real space taking $q \rightarrow -i\partial_z$ in Eq. (67). To include SC order we then follow the same path that led us to Eq. (35) and obtain the BdG Hamiltonian relevant to this situation

$$H_{\text{BdG}} = v(-i\partial_z)\sigma^y\tau^z + m(z)\sigma^x + \Delta(z)\tau^x, \quad (68)$$

where we have set $\mu = 0$ and assumed that $\Delta(z)$ is real. To find the expected Majorana zero mode we seek a zero-energy eigenstate $H_{\text{BdG}}\Phi_0(z) = 0$ in the vicinity of a domain wall between SC and magnetic domains, as illustrated in Fig. 8c. It is a simple matter to show that there exists precisely one such zero mode with the wavefunction

$$\Phi_0(z) = \frac{\chi_0(z)}{\sqrt{2}} \begin{pmatrix} 0 \\ 1 \\ -1 \\ 0 \end{pmatrix}, \quad \chi_0(z) = Ae^{-\frac{1}{v} \int_0^z dz' [m(z') - \Delta(z')]}, \quad (69)$$

where A is a normalization constant. The corresponding field operator takes the form

$$\hat{\psi}_0 = \frac{1}{\sqrt{2}} \int dz \chi_0(z) [c_\downarrow(z) + c_\downarrow^\dagger(z)], \quad (70)$$

and obeys the requisite Majorana condition $\hat{\psi}_0^\dagger = \hat{\psi}_0$. We note that the other domain wall (with SC domain to the right of the magnetic domain) also hosts a Majorana zero mode which involves spin-up electrons. Also, we remark that Majorana zero modes persist for an arbitrary complex order parameter Δ and for chemical potential $|\mu| < |m|$, although the solution is slightly more complicated when $\mu \neq 0$ with the wavefunction $\Phi_0(z)$ oscillating at the relevant Fermi wavevector.

This proposal is elegant in its simplicity but unfortunately of the known 2D topological insulators (HgTe and InAs quantum wells) neither is particularly well suited for the experimental realization of the requisite setup Fig 8a. The problem lies mainly in interfacing the edge, which tends to be buried inside a complicated heterostructure, with a superconductor and a ferromagnet, as well as the general paucity of suitable insulating ferromagnets. Simpler realizations of 2D TIs in physical systems with easily accessible edges would clearly further the goal of realizing Majorana fermions based on this construction.

2. Nanowire made from a 3D topological insulator

The surface of a 3D topological insulator, such as Bi_2Se_3 and Bi_2Te_3 , is known to host a single gapless linearly dispersing Dirac fermion. The massless character of this surface state is protected by \mathcal{T} . For a planar surface perpendicular to the z axis the low-energy theory of the Dirac mode is described by the Bloch Hamiltonian (Hasan and Kane, 2010)

$$h_0(\mathbf{q}) = v(q_x \sigma^y - q_y \sigma^x) - \mu. \quad (71)$$

We shall be interested in a quasi-1D wire geometry, illustrated in Fig. 9a. The wire exhibits Majorana end-modes when it is threaded by magnetic flux of half-integer flux quanta and brought into proximity of a superconductor (Cook and Franz, 2011). To see this we note that a Dirac Hamiltonian analogous to Eq. (71) can

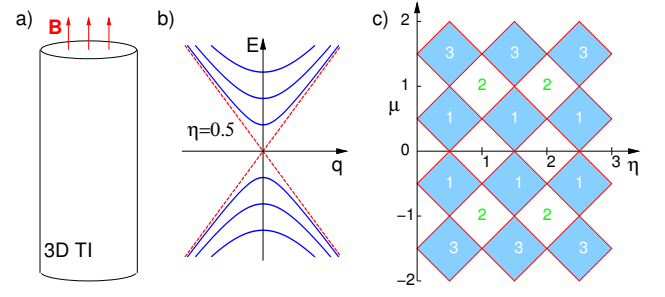


FIG. 9 a) 3D topological insulator wire in longitudinal magnetic field \mathbf{B} . b) Spectrum of the surface state excitations when the total flux piercing the wire $\eta = \Phi/\Phi_0 = SB/\Phi_0$ is half-integer. The dashed lines indicate non-degenerate bands while those represented by the solid lines are doubly degenerate. c) The topological phase diagram in the limit of small Δ . Shaded regions represent the topological phase and the numerals indicate the number of Fermi points in the right half of the Brillouin zone.

be formulated for an arbitrary curved surface (Ostrovsky *et al.*, 2010) and solved exactly for a surface of an infinitely long cylindrical wire with radius R threaded by magnetic flux Φ (Rosenberg *et al.*, 2010). The solution, details of which are unimportant for our purposes, yields an excitation spectrum of the form

$$\epsilon_l(q_z) = \pm v \hbar \sqrt{q_z^2 + \left(\frac{l + \eta - 1/2}{R} \right)^2}, \quad (72)$$

where q_z is the momentum along the axis of the cylinder, $l = 0, \pm 1, \dots$ is the angular momentum and $\eta = \Phi/\Phi_0$ is the magnetic flux in units of flux quantum $\Phi_0 = hc/e$. The $\frac{1}{2}$ offset in the angular momentum comes from the Berry phase associated with the 2π rotation of the electron spin as it encircles the cylinder and implies finite-size gap $v\hbar/R$ in the absence of magnetic field. In addition, all levels are doubly degenerate in this case. A more interesting situation arises when η is half-integer (e.g. when $\Phi = \frac{1}{2}\Phi_0$). In this case the Berry phase offset is canceled and, as a result, a single non-degenerate gapless branch arises of the form $\pm v\hbar q_z$, while all other branches remain doubly degenerate. This situation is illustrated in Fig. 9b. The spectrum now exhibits an odd number of Fermi points in the right half of the Brillouin zone when the chemical potential resides inside the bulk bandgap and we expect a topological state to emerge when superconductivity is induced. The resulting topological phase diagram is depicted in Fig. 9c.

When the chemical potential is small, $|\mu| < v\hbar/2R$, so that it intersects only the lowest band, one can easily solve for the Majorana zero modes. The procedure is essentially identical to the one discussed above for the edge of the 2D TI and yields a Majorana zero mode at each end of the wire. When more bands are occupied then the solution becomes more involved but preserves the Majorana modes up until the chemical potential reaches the bulk

bands. For wires with a rectangular cross section, such as those grown experimentally, the formula (72) for the normal state spectrum holds only approximately but the pattern of degeneracies (i.e. one gapless non-degenerate branch plus a set of gapped doubly degenerate bands) remains robust as a consequence of \mathcal{T} -invariance. One thus expects Majorana zero modes to exist in this case as well and this is indeed confirmed by numerical calculations (Cook and Franz, 2011; Cook *et al.*, 2012).

The present setup has potential advantages over the edge of a 2D TI: (i) nanowires can be readily contacted by a superconductor and (ii) since Majorana zero modes occur at the ends no insulating ferromagnets are required (the requisite \mathcal{T} breaking is provided by magnetic flux lines entering and exiting the wire). Despite these potential advantages Majorana zero modes have not yet been observed in TI nanowires. Some encouraging results towards their realization will be discussed in Sec. IV.

3. Semiconductor quantum wires

Another platform for Majorana fermions is based on ordinary semiconductors with strong spin-orbit coupling (SOC), as realized by InSb or InAs. This platform has gained a significant momentum recently due to the existing expertise and technological background available for these long studied materials. The initial proposal involved a 2D structure composed of semiconductor and superconductor films interfaced with an insulating ferromagnet (Sau *et al.*, 2010) or in the presence of external in-plane magnetic field (Alicea, 2010). Later, advantages of 1D quantum wires have been recognized (Lutchyn *et al.*, 2010; Oreg *et al.*, 2010) and this is now the leading solid-state candidate for the experimental realization of unpaired Majorana zero modes. We shall focus on this system.

To understand the physics behind this proposal we start from a Hamiltonian describing the low-energy electrons in a 1D quantum wire with a Rashba SOC,

$$\mathcal{H}(q_z) = \frac{\hbar^2 q_z^2}{2m_{\text{eff}}} + \alpha \hat{\mathbf{n}} \cdot (\boldsymbol{\sigma} \times \mathbf{q}). \quad (73)$$

Here m_{eff} is the electron effective mass, α sets the strength of the SOC, and $\hat{\mathbf{n}}$ its direction. For a quantum wire supported by a substrate, $\hat{\mathbf{n}}$ points in the direction perpendicular to the substrate surface, which we take at $y = 0$. In this case the SOC takes the form $\alpha \sigma^x q_z$. The spectrum of excitations is comprised of two shifted parabolas,

$$\epsilon(q_z) = \frac{\hbar^2 q_z^2}{2m_{\text{eff}}} \pm \alpha q_z, \quad (74)$$

and is depicted in Fig. 10a. It is seen that SOC separates the two spin projections but there is still an even number of Dirac points in the right half of the Brillouin zone for any chemical potential. To change this one must

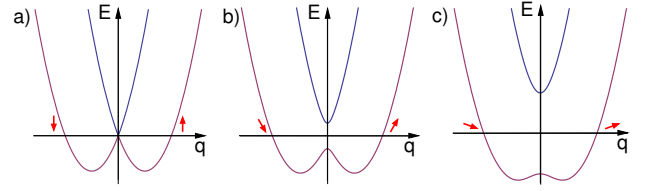


FIG. 10 Excitation spectra of a single channel semiconductor quantum wire Eq. (74). The three panels show representative cases with different Zeeman coupling, a) $V_Z/E_{\text{SO}} = 0.0$, b) 0.4 and c) 1.2. The red arrows indicate the spin direction at the Fermi points.

in addition apply a magnetic field \mathbf{B} . If its direction is perpendicular to x then a gap opens up in the spectrum (74) at $q_z = 0$ due to the Zeeman coupling, as illustrated in Fig. 10b. Specifically, for the field along z the perturbation reads

$$\delta\mathcal{H} = V_Z \sigma^z \quad (75)$$

and the spectrum becomes

$$\epsilon(q_z) = \frac{\hbar^2 q_z^2}{2m_{\text{eff}}} \pm \sqrt{\alpha^2 q_z^2 + V_Z^2}, \quad (76)$$

When the chemical potential is tuned to lie inside the Zeeman gap, $|\mu| < V_Z$, then the system exhibits a single Fermi point for $q_z > 0$ and we expect it to enter the topological phase upon inducing the SC order. In the presence of a superconducting gap Δ the Kitaev criterion Eq. (63) imposes

$$\sqrt{\mu^2 + \Delta^2} < V_Z \quad (77)$$

as a condition for the topological state. An explicit calculation once again confirms the existence of an unpaired Majorana mode at the end of the wire in this regime but we shall not reproduce it here.

As already mentioned this proposal has attracted by far the most attention from theorists and experimentalists alike and as a result much is known about this system beyond the simplest model outlined above. Among the key experimentally relevant issues are the effect of multiple bands (arising from the fact that real wires are not truly one-dimensional systems) and disorder, which is generically present in any solid state system, as well as details of the proximity effect for specific materials. Existing literature devoted to these issues has been reviewed in recent articles (Alicea, 2012; Beenakker, 2013a; Stanescu and Tewari, 2013). In the present article we shall not attempt to give a comprehensive review but merely outline some key challenges facing this proposal in comparison to those mentioned previously. An interested reader is referred to the above mentioned review articles for more in-depth discussion.

A key quantity to consider is the Zeeman gap V_Z because according to Eq. (77) its magnitude limits the size

of the excitation gap in the system and sets the window for the chemical potential μ . For electrons in a solid $V_Z = g\mu_B B$ where g is the relevant g factor and $\mu_B = 5.788$ eV/T is the Bohr magneton. Both InAs and InSb exhibit large g factors (15 and 50, respectively) and in a typical laboratory field of 0.1T this translates to $V_Z \simeq 1 - 10$ K. One immediately obvious challenge is therefore to tune the chemical potential μ to within a window just several Kelvins wide. It is also clear from Eq. (77) that the proximity induced SC gap Δ must be smaller than this scale so the experiments must be performed at mK temperatures. One obvious route to improving the situation is to apply stronger magnetic fields. Magnetic fields that are too high, however have a potential to destroy SC order in the substrate. They also have a more subtle effect of reducing the induced SC gap Δ due to spin canting. To see this we have to consider the energy scale associated with SOC, $E_{\text{SO}} = \frac{1}{2}m_{\text{eff}}\alpha^2$ which is typically of order 1K in both InAs and InSb. When $E_{\text{SO}} \gg V_Z$ then the electron spins near the opposite Fermi points are essentially anti-aligned, and are thus naturally susceptible to the formation of spin-singlet Cooper pairs. In the opposite limit, however, the two spins are pointing in essentially the same direction (set by the field \mathbf{B}), Fig. 10c, and spin-singlet pairing is strongly suppressed: one is, in essence, trying to induce SC order in a ferromagnet. Thus, attempts to increase V_Z without simultaneously adjusting E_{SO} are met with diminishing returns. The strength of SOC is to some extent tunable although it is largely controlled by the material properties and the system geometry.

Another set of constraints arises from the inevitable disorder that is present both in the wire and in the SC substrate. The effect of disorder is twofold. First, even though the average chemical potential $\bar{\mu}$ may be tuned to within the Zeeman gap, disorder induced fluctuations $\delta\mu$ may drive segments of the wire out of the topological phase. Second, in a system with broken \mathcal{T} disorder is known to suppress the size of the SC gap. This makes the Majorana zero modes more difficult to observe because of the increased demand for the experimental energy resolution. They are also more susceptible to thermal fluctuations. It is worth mentioning at this point that the challenges mentioned here are thought to be much diminished in the proposals involving topological insulators in 2D and 3D reviewed in previous subsections. This is because in those systems chemical potential must only be tuned to within the bulk bandgap, which is tens of Kelvins in HgTe quantum wells and ~ 300 meV in 3D topological insulators like Bi₂Se₃. Also, the underlying normal metal is \mathcal{T} -invariant, which alleviates problems related to disorder.

Despite various challenges, semiconductor nanowires proximity coupled to superconductors are currently farthest along in terms of experimental realization of Majorana fermions. We shall give a brief review of the existing experimental studies in Sec. IV and provide a critical discussion of the claims that Majorana fermions have been

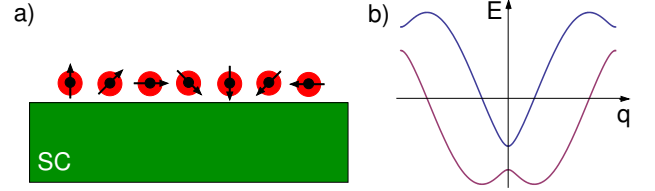


FIG. 11 a) Chain of magnetic atoms deposited on a SC substrate. The arrows indicate the direction of atomic magnetic moments. b) Excitation spectrum of electrons in such a chain for $JS = 0.07t$ and the angle between neighboring magnetic moments $\pi/2$.

already observed in these systems.

4. Helical spin chains

In the proposals discussed thus far spin-orbit coupling played an essential role in giving rise to a normal state with spin degeneracy removed. SOC is fundamentally a relativistic effect and this is the main reason why the associated energy scales remain relatively small in solid state systems. We close this subsection with a description of a simple system that can host Majorana fermions but does not rely on SOC. Consider a chain of magnetic atoms, such as Gd, Cr or Fe, deposited on an atomically flat SC substrate. Each such magnetic moment is known to create a bound state with the energy inside the SC gap, known as the Shiba state (Shiba, 1968). The distance between the magnetic atoms is chosen such that the bound-state wavefunctions have a significant overlap t . It turns out that the magnetic moments \mathbf{S}_j of the atoms in this situation have a tendency to order in a co-planar spiral. As we illustrate below the 1D electron system formed of the hybridized Shiba states can be in the topological phase with unpaired Majorana fermions localized at its ends (Choy *et al.*, 2011; Martin and Morpurgo, 2012; Nadj-Perge *et al.*, 2013).

To see how this comes about we write down the simplest Hamiltonian describing the 1D system discussed above. It consists of electrons hopping along the chain and coupled to magnetic moments,

$$\begin{aligned} \mathcal{H} = & - \sum_{ij\sigma} t_{ij} c_{i\sigma}^\dagger c_{j\sigma} - \mu \sum_{i\sigma} c_{i\sigma}^\dagger c_{i\sigma} \\ & + J \sum_i \mathbf{S}_i \cdot (c_{i\sigma}^\dagger \boldsymbol{\sigma}_{\sigma\sigma'} c_{i\sigma'}) + \sum_j (\Delta c_{j\uparrow}^\dagger c_{j\downarrow}^\dagger + \text{h.c.}), \end{aligned} \quad (78)$$

where J stands for the exchange coupling constant and the last term represents the proximity-induced SC order. We consider a co-planar helical arrangement of atomic spins as indicated in Fig. 11a,

$$\mathbf{S}_j = S[\cos(Gx_j), \sin(Gx_j), 0] \quad (79)$$

where G is the corresponding wavevector and the chain is assumed to lie along the x -axis. We note that Hamiltonian (78) is invariant under the simultaneous global

SU(2) rotation of the electron and atomic spins so the solution below applies to any co-planar spiral.

To find the spectrum of excitations it is expedient to perform a spin-dependent gauge transformation (Martin and Morpurgo, 2012),

$$c_{j\uparrow} \rightarrow c_{j\uparrow} e^{\frac{i}{2} G x_j}, \quad c_{j\downarrow} \rightarrow c_{j\downarrow} e^{-\frac{i}{2} G x_j}. \quad (80)$$

Upon this transformation the Hamiltonian becomes translation invariant and can be written in the momentum space as follows,

$$\begin{aligned} \mathcal{H} = \sum_q & \left[\xi(q) c_{q\sigma}^\dagger c_{q\sigma} + b(q) c_{q\sigma}^\dagger \sigma_{\sigma\sigma'}^z c_{q\sigma'} \right. \\ & \left. + JS c_{q\sigma}^\dagger \sigma_{\sigma\sigma'}^x c_{q\sigma'} + (\Delta c_{q\uparrow}^\dagger c_{-q\downarrow}^\dagger + \text{h.c.}) \right]. \end{aligned} \quad (81)$$

In the above

$$\begin{aligned} \xi(q) &= \frac{1}{2} [\epsilon_0(q - G/2) + \epsilon_0(q + G/2)] - \mu, \\ b(q) &= \frac{1}{2} [\epsilon_0(q - G/2) - \epsilon_0(q + G/2)], \end{aligned} \quad (82)$$

with $\epsilon_0(q) = \sum_j t_{0j} e^{iqx_j}$ the normal-state dispersion in the absence of the exchange coupling. For nearest-neighbor hopping $\epsilon_0(q) = -2t \cos q$. The transformed Hamiltonian (81) now can be identified as a lattice version of the Hamiltonian describing the semiconductor quantum wire discussed in the previous subsection with JS and $b(q)$ playing the role of the Zeeman field and SOC, respectively. Its normal state spectrum is given by

$$\epsilon(q) = \xi(q) \pm \sqrt{b(q)^2 + J^2 S^2}, \quad (83)$$

which should be compared with Eq. (76). For nearest-neighbor hopping the characteristic spectrum is depicted in Fig. 11b. We see that when

$$|\mu \pm 2t \cos G/2| < JS \quad (84)$$

the system satisfies the Kitaev criterion and should be in the topological phase once SC order is induced by the proximity effect.

It is clear from the foregoing discussion that the existence of Majorana fermions in this proposal relies in a crucial way on the formation of the spiral spin state with the correct pitch G . For a given chemical potential μ the latter must satisfy Eq. (84) for the topological state to emerge. The spiral state and its stability against fluctuations and interactions has been studied in recent theoretical works (Braunecker and Simon, 2013; Klinovaja *et al.*, 2013; Pientka *et al.*, 2013; Vazifeh and Franz, 2013) with some encouraging results. The main finding is that for energetic reasons the spiral pitch G selfconsistently adjusts to the changing chemical potential so that the system remains in the topological phase. In addition, this ‘self-organized’ topological state appears stable against the effects of fluctuations and interactions.

Structures composed of single atoms such as the 1D chain discussed here can now be built fairly routinely using techniques of scanning tunneling microscopy (Gomes *et al.*, 2012). The first attempt to construct the present system has been recently reported with some encouraging results and will be discussed in Sec. IV.

D. Systems in two dimensions

An important property of the solid-state realizations of Majorana particles in two dimensions is their non-trivial exchange statistics. This property is thought to harbor a unique potential for future applications in quantum computation in which operations would be topologically protected against the effects of decoherence. The recent surge of interest in Majorana fermions owes much to these prospects and the aim of this subsection is to explain the physics behind the phenomenon of non-Abelian exchange statistics as realized in simple models of 2D topological superconductors.

1. Non-Abelian exchange statistics: general considerations

As noted before a pair of spatially separated Majorana fermions γ_{j1}, γ_{j2} can be thought of as forming one ordinary Dirac fermion represented by creation and annihilation operators c_j^\dagger, c_j defined in Eq. (10). Let us imagine that we have $2N$ such well-separated Majorana particles arranged in a 2D plane. We also assume that there are no other low-energy degrees of freedom in this region of space, i.e. our Majorana zero modes are protected by a minigap. It is easy to see that the ground state of this system exhibits a 2^N -fold degeneracy⁵ arising from two possible occupancies $n_j = 0, 1$ of each of the N ordinary fermion states. The corresponding degenerate Hilbert space is spanned by basis vectors

$$|\Phi_{\{n_j\}}\rangle = |n_1, n_2, \dots, n_N\rangle, \quad (85)$$

where n_j denotes the eigenvalue of the corresponding number operator

$$\hat{n}_j = c_j^\dagger c_j = \frac{1}{2} (1 + i\gamma_{j1}\gamma_{j2}). \quad (86)$$

The state vector $|\Psi\rangle$ composed of an arbitrary linear combination of the basis vectors $|\Phi_{\{n_j\}}\rangle$ can be used to encode quantum information.

This way of encoding quantum information has two important advantages compared to many other schemes. First, as can be seen from the definition of the number

⁵ In reality the degeneracy is only 2^{N-1} because of the electron parity considerations. $\nu = (\sum_j n_j) \bmod 2$ represents the electron parity which is conserved in a fully gapped, isolated superconductor.

operator in Eq. (86), the information in each quantum bit is stored *nonlocally*. In order to read the information one must either bring the constituent Majorana particles close together (to test if the combined fermionic state is filled or empty by a local measurement) or else perform a coherent measurement at two distant spatial positions. On the other hand it is clear that no local measurement of a single Majorana fermion can access the stored information. Since the environment presumably cannot perform a non-local measurement, the information stored in the quantum bit \hat{n}_j is thought to be immune to the effects of decoherence. One caveat here is that if there exist uncontrolled low-energy excitations in the system then the environment can potentially flip the quantum bit (without reading it) by tunneling a fermion into the qubit – this is possible even if only one Majorana can be accessed. The existence of the minigap is therefore crucial for preserving the quantum information stored in a pair of Majorana zero modes.

The second key feature of the setup described above is the ability to manipulate the quantum information stored in $|\Psi\rangle$ in a topologically protected fashion. As we will demonstrate below *braiding* of Majorana fermions – performing adiabatic exchanges of their positions – implements certain unitary transformations on the state vector $|\Psi\rangle$. The corresponding braid group turns out to be non-Abelian, meaning that unitary transformations describing individual exchanges do not in general commute. A sequence of exchanges performed on a properly initialized quantum state $|\Psi_i\rangle$ followed by a readout of the final state $|\Psi_f\rangle$ thus constitutes a topologically protected quantum computation. Unfortunately, it is known that the braid group realized by exchanging Majorana fermions is not sufficiently rich to perform an arbitrary unitary transformation on $|\Psi_i\rangle$ which would be needed to implement a universal quantum computer. To achieve the latter the braid group must be supplemented by some ‘unprotected’ operations making the system vulnerable to decoherence, although in theory much less so than a non-topological quantum computer (Nayak *et al.*, 2008).

Majorana fermions with the above non-Abelian exchange statistics have been theoretically proposed to exist in a number of 2D systems. Historically the first was the so called Moore-Read Pfaffian state (Moore and Read, 1991) that many believe describes the fractional quantum Hall state observed at $\nu = \frac{5}{2}$ filling. Another is the thin film of a spin-polarized $p_x + ip_y$ superconductor, which may be realized in Sr_2Ru_3 , although definitive evidence for this pairing state is still lacking (Kallin, 2012). More recently Fu and Kane proposed that a 2D topological superconductor with the requisite properties could arise at an interface formed between a 3D topological insulator and a conventional s -wave superconductor (Fu and Kane, 2008). Majorana zero modes are expected to be localized in the cores of Abrikosov vortices in such a 2D superconductor. In the following we shall focus on this model because it is closest in the spirit to our previous discussions and also because it might be most

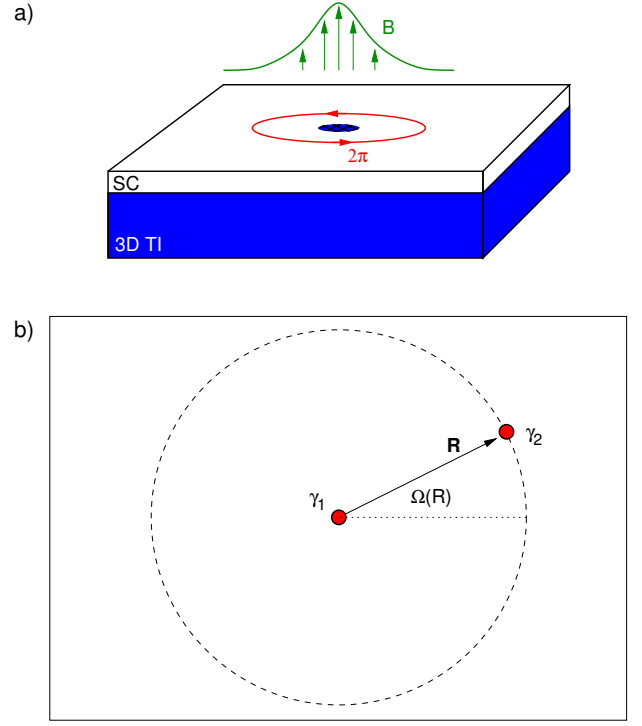


FIG. 12 a) Schematic setup for the Fu-Kane model with a 3D TI covered with a thin layer of SC film. A vortex is depicted in the surface layer with a small core, phase winding 2π and a sketch of a magnetic field profile $B(\mathbf{r})$. b) Vortex with Majorana fermion γ_2 encircles a vortex placed at the origin with Majorana γ_1 in its core.

amenable to various practical tests of non-Abelian exchange statistics. Although the underlying mathematics differs in some details, the key aspects of the physics describing the $p_x + ip_y$ superconductor and the Moore-Read Pfaffian state are the same (Read and Green, 2000).

2. Vortices in Fu-Kane model

Fu and Kane (Fu and Kane, 2008) envisioned inducing superconductivity in the surface state of a 3D topological insulator by covering it in with a thin film of an ordinary s -wave superconductor such as Pb or Nb as depicted in Fig. 12a. Although more elaborate treatments are possible the simplest model that captures the essential physics of this situation consists of a Hamiltonian h_0 describing the TI surface defined in Eq. (71) with the superconducting order included via the BdG formalism described in Sec. IV.A. The resulting BdG Hamiltonian (35) can be written in the following form

$$H_{\text{BdG}}(\mathbf{r}) = \begin{pmatrix} 0 & p_- & \Delta(\mathbf{r}) & 0 \\ p_+ & 0 & 0 & \Delta(\mathbf{r}) \\ \Delta^*(\mathbf{r}) & 0 & 0 & -p_- \\ 0 & \Delta^*(\mathbf{r}) & -p_+ & 0 \end{pmatrix}, \quad (87)$$

where $p_{\pm} = p_x \pm ip_y$, and we have set $v = 1$ and $\mu = 0$ for the sake of simplicity.

We are interested in finding the eigenstates of $H_{\text{BdG}}(\mathbf{r})$ in the presence of an Abrikosov vortex. For our purposes the vortex is defined as a point around which the phase of $\Delta(\mathbf{r})$ winds by $2\pi n$ with n integer. More generally, an isolated Abrikosov vortex also requires a magnetic flux $hc/2e$ spread in a flux tube with a characteristic size $\lambda \simeq 10 - 10^3 \text{\AA}$ around the vortex center (Fig. 12a). However, inclusion of the magnetic flux is unimportant for the existence of the Majorana zero mode and we shall henceforth neglect it. For a vortex placed at the origin we thus have

$$\Delta(\mathbf{r}) = \Delta_0(r)e^{-i(n\varphi+\alpha)}, \quad (88)$$

where $\Delta_0(r)$ is a real function of the distance, φ represents the polar angle and α denotes an arbitrary constant phase offset that will become important in our later discussion of vortex braiding. Single-valuedness of the Hamiltonian dictates that for n nonzero $\Delta_0(r)$ vanishes at the origin. Energy considerations further show that $\Delta_0(r) \sim r^{|n|}$ for small r but this is not essential for our considerations.

To find the zero modes of $H_{\text{BdG}}(\mathbf{r})$ in the presence of a vortex it is useful to first perform a unitary transformation $H_n = UH_{\text{BdG}}U^{-1}$ with

$$U = \begin{pmatrix} 1 & 0 & 0 & 0 \\ 0 & 0 & 0 & 1 \\ 0 & 0 & 1 & 0 \\ 0 & 1 & 0 & 0 \end{pmatrix}, \quad (89)$$

which brings the Hamiltonian into the following off-diagonal form

$$H_n = \begin{pmatrix} 0 & D_n \\ D_n^\dagger & 0 \end{pmatrix}. \quad (90)$$

The transformed Hamiltonian acts on the Nambu spinor $\hat{\Psi}_{\mathbf{r}} = (c_{\uparrow\mathbf{r}}, c_{\uparrow\mathbf{r}}^\dagger, -c_{\downarrow\mathbf{r}}, c_{\downarrow\mathbf{r}})^\top$ and

$$D_n = \begin{pmatrix} \Delta(\mathbf{r}) & p_- \\ -p_+ & \Delta^*(\mathbf{r}) \end{pmatrix}. \quad (91)$$

Passing into the polar coordinates and making use of the identity $p_{\pm} = e^{\pm i\varphi}(-i\partial_r \pm r^{-1}\partial_\varphi)$ we may write

$$D_n = \begin{pmatrix} e^{-i(n\varphi+\alpha)}\Delta_0(r) & e^{-i\varphi}(-i\partial_r - \frac{\partial_\varphi}{r}) \\ -e^{i\varphi}(-i\partial_r + \frac{\partial_\varphi}{r}) & e^{i(n\varphi+\alpha)}\Delta_0(r) \end{pmatrix}. \quad (92)$$

When looking for the zero modes the off-diagonal form of the Hamiltonian (90) has a distinct advantage: the zero modes necessarily have the spinor structure $(\psi(\mathbf{r}), 0)^T$ and $(0, \chi(\mathbf{r}))^T$ where $\psi(\mathbf{r})$ and $\chi(\mathbf{r})$ are two-component zero modes of D_n^\dagger and D_n respectively. For a positive singly quantized vortex ($n = 1$) it is easy to show that there exists a normalizable zero mode of D_1 of the form

$$\chi(\mathbf{r}) = \frac{1}{\sqrt{2}} \begin{pmatrix} e^{-i(\alpha/2-\pi/4)} \\ e^{i(\alpha/2-\pi/4)} \end{pmatrix} f_0(r), \quad (93)$$

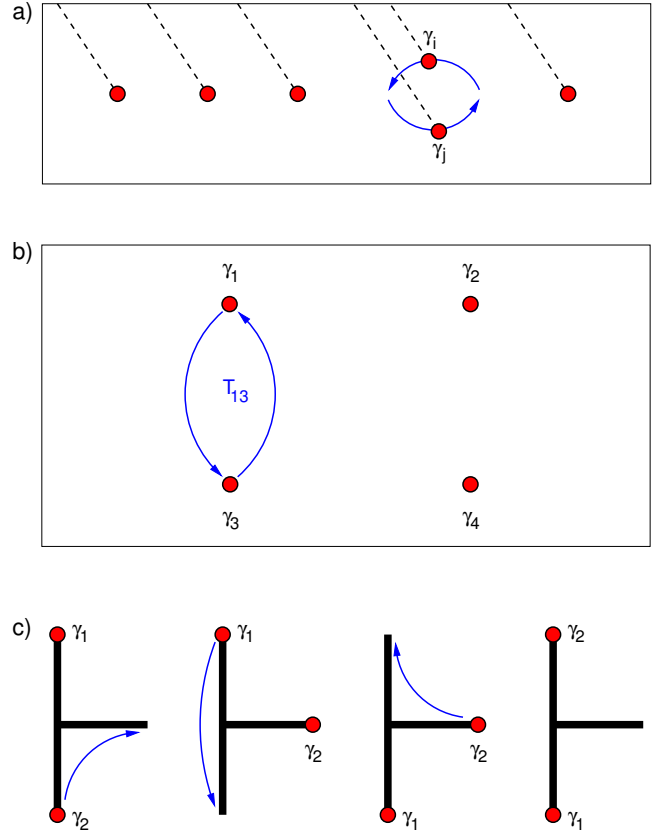


FIG. 13 a) Upon exchange of two Majoranas one of them must cross the branch cut implied by the wavefunction Eq. (96). When the branch cuts are chosen as indicated by the dashed lines then counterclockwise exchange of γ_i and γ_j results in rules summarized in Eq. (101). b) Setup used for the demonstration of the simplest topologically protected operations on the internal Hilbert space spanned by $|n_a, n_b\rangle$. c) Exchange of two Majorana particles in a T-junction formed by interconnected 1D wires.

with $f_0(r) = Ae^{-\int_0^r \Delta_0(r')dr'}$, while D_1^\dagger does not have a normalizable zero mode. The field operator of the zero mode can be constructed following Eq. (48) and reads

$$\hat{\psi}_0 = \frac{i}{\sqrt{2}} \int d^2r \left[e^{i(\alpha/2-\pi/4)} c_{\mathbf{r}\downarrow} - e^{-i(\alpha/2-\pi/4)} c_{\mathbf{r}\downarrow}^\dagger \right] f_0(r). \quad (94)$$

As expected, the zero mode represents a Majorana particle. We note that a singly quantized antivortex ($n = -1$) also possesses a zero mode, this time in the upper component of the spinor $\psi(\mathbf{r})$ and the corresponding Majorana field operator Eq. (94) is then composed of a spin-up electron and a spin-up hole.

3. Vortex exchange and braiding

Having established the existence of a Majorana zero mode in the core of a vortex in the Fu-Kane model we now proceed to discuss their statistics under exchange.

These results follow from the earlier studies (Moore and Read, 1991; Read and Green, 2000) but we follow the physically more transparent derivation given by Ivanov (Ivanov, 2001). Although exact analytical solutions are not available for a system of many vortices it is reasonable to assume that a single Majorana mode will continue to exist in the core of each vortex as long as these are well separated compared to the zero mode size $\xi = v/\Delta_0$ where Δ_0 is the SC gap in the absence of vortices.

We begin by considering the effect of a vortex encircling another vortex located at the origin. If their distance $d \gg \xi$ we can neglect the exponentially small splitting of the zero mode energies resulting from the wavefunction overlap and the only effect will be the change of SC phase near the origin due to the phase field produced by the distant vortex. In view of Eq. (88) and by inspecting Fig. 12b this phase change can be expressed as

$$\alpha(\mathbf{R}) = \alpha_0 + \Omega(\mathbf{R}) + \pi \quad (95)$$

where $\Omega(\mathbf{R})$ is the polar angle of the distant vortex and α_0 denotes an arbitrary constant phase offset that we can adjust at will without affecting the physics. (The latter corresponds to the global U(1) phase of the condensate and does not have physical meaning.) Taking $\alpha_0 = -\frac{\pi}{2}$ the wavefunction (93) of the Majorana mode at the origin becomes

$$\chi_{\mathbf{R}}(\mathbf{r}) = \frac{1}{\sqrt{2}} \left(e^{-\frac{i}{2}\Omega(\mathbf{R})} \right) f_0(r), \quad (96)$$

where the subscript \mathbf{R} reminds us that the wavefunction now depends on the position of the distant vortex.

As the distant vortex adiabatically encircles the origin counterclockwise over the time interval $t \in (0, T)$ the Majorana wavefunction $\chi(\mathbf{r}, t)$ acquires a Berry phase through the dependence of the instantaneous eigenstate $\chi_{\mathbf{R}(t)}(\mathbf{r})$ on the time parameter. The Berry phase reads

$$\gamma(\mathcal{C}) = -\text{Im} \oint_{\mathcal{C}} \langle \chi_{\mathbf{R}} | \nabla_{\mathbf{R}} \chi_{\mathbf{R}} \rangle \cdot d\mathbf{R} - i \ln [\langle \chi_{\mathbf{R}(0)} | \chi_{\mathbf{R}(T)} \rangle], \quad (97)$$

where the second term must be included in order to account for the fact that $\chi_{\mathbf{R}}(\mathbf{r})$ as defined in Eq. (96) is not single valued as $\Omega \rightarrow \Omega + 2\pi$. An explicit evaluation shows that the first term vanishes but the second term yields $\gamma(\mathcal{C}) = \pi$. This leads to the conclusion that upon being encircled by another singly quantized vortex the Majorana zero mode wavefunction *changes its sign*. This is a direct consequence of the wavefunction being an equal superposition of an electron and a hole, which acquire a phase of $+\pi$ and $-\pi$ respectively upon the adiabatic change in the order parameter phase by 2π .

The Majorana wavefunction of the distant vortex also changes sign because its local SC phase likewise advances by 2π . If we denote the Majorana operators corresponding to the two vortices by γ_1 and γ_2 then the effect of the encircling operation can be encoded as

$$\gamma_1 \mapsto -\gamma_1, \quad \gamma_2 \mapsto -\gamma_2. \quad (98)$$

For a set of $2N$ Majorana modes γ_k an operation in which γ_j encircles γ_i can be implemented by a unitary transformation

$$\gamma_k \mapsto U_{ij} \gamma_k U_{ij}^\dagger, \quad U_{ij} = \gamma_i \gamma_j. \quad (99)$$

An adiabatic exchange of two Majoranas γ_i and γ_j can be thought of as a half of the encircling operation (two subsequent counterclockwise exchanges are equivalent to a single counterclockwise encircling operation). The unitary operator implementing such an exchange is therefore

$$T_{ij} = (U_{ij})^{1/2} = \frac{1}{\sqrt{2}} (1 + \gamma_i \gamma_j). \quad (100)$$

Applying this unitary transformation we find the following rule governing such pairwise exchanges

$$\gamma_i \mapsto -\gamma_j, \quad \gamma_j \mapsto \gamma_i, \quad \gamma_k \mapsto \gamma_k, \quad (101)$$

for $k \neq i, j$. These rules, first derived in this form by Ivanov (Ivanov, 2001), can be intuitively understood by appealing to Fig. 13a. The form of T_{ij} given in Eq. (100) also belies the non-Abelian structure of the braid group; it is easy to check that subsequent exchanges do not in general commute, e.g. $T_{12}T_{23} \neq T_{23}T_{12}$.

We close this subsection by working out a simple example that nicely illustrates the action of the above derived transformations on specific quantum states. Consider a system with 4 Majorana particles $\gamma_1, \gamma_2, \gamma_3$, and γ_4 localized in vortices and arranged as indicated in Fig. 13b. Of these we form two ordinary fermions

$$c_a = \frac{1}{2}(\gamma_1 + i\gamma_2), \quad c_b = \frac{1}{2}(\gamma_3 + i\gamma_4), \quad (102)$$

and label the resulting two-dimensional Hilbert space by the eigenvalues of the corresponding number operators $|n_a, n_b\rangle$. Let us consider the action of several operations on this state. Encircling γ_3 by γ_1 is implemented by $U_{31} = \gamma_3 \gamma_1 = (c_a^\dagger + c_a)(c_b^\dagger + c_b)$ and gives

$$|n_a, n_b\rangle \mapsto U_{31}|n_a, n_b\rangle = (-1)^{n_a} |\bar{n}_a, \bar{n}_b\rangle, \quad (103)$$

where $\bar{n} = (1 - n) \bmod 2$ denotes a state with opposite occupancy to n . The encircling operation performed between the constituent members of different fermions thus reverses the occupancy of the states, e.g. $|0, 0\rangle \mapsto |1, 1\rangle$ or $|1, 0\rangle \mapsto -|0, 1\rangle$. Meanwhile encircling between the Majorana members of the same fermion just changes the overall sign of the state vector.

One can similarly work out the effect of exchanges, for instance

$$\begin{aligned} T_{12}|n_a, n_b\rangle &= e^{i\frac{\pi}{4}(1-2n_a)} |n_a, n_b\rangle \\ T_{31}|n_a, n_b\rangle &= \frac{1}{\sqrt{2}} (|n_a, n_b\rangle + (-1)^{n_a} |\bar{n}_a, \bar{n}_b\rangle), \end{aligned} \quad (104)$$

We observe that exchanging two Majoranas belonging to the same fermion c merely attaches an (occupancy dependent) overall phase factor to the state. Exchange

of Majoranas belonging to different fermions, however, creates an new entangled state. The set of operations afforded by the braid group allows for non-trivial manipulations of the ground-state degenerate manifold but unfortunately does not permit creation of an arbitrary state $|\Psi\rangle = \sum_{n_a, n_b} C_{n_a, n_b} |n_a, n_b\rangle$ from a given reference state by repeated application of group elements T_{ij} . As a result this system cannot be used to perform a generic quantum computation. There exist, however, theoretical proposals for solid state realizations of emergent particles with more complicated non-Abelian statistics, e.g. the so called “Fibonacci anyons”, whose braid group is sufficiently rich to permit construction of a universal quantum computer (Nayak *et al.*, 2008).

To conclude this Section we reiterate that vortices in spin-polarized $p_x + ip_y$ superconductor and quasiparticles in the Moore-Read Pfaffian state can be treated in a fashion similar to our preceding discussion. The corresponding analysis shows that Majorana fermions in those systems obey non-Abelian exchange statistics described by the same braid group. Similar situation arises also in artificially engineered 2D heterostructures combining ordinary superconductors, semiconductors with strong SOC and magnetic insulators (Alicea, 2010; Sau *et al.*, 2010). All these systems realize the same 2D topological phase which hosts Majorana particles with non-Abelian exchange statistics.

Our discussion of 2D systems naturally motivates the following question: What is the exchange statistics of Majorana particles in 1D structures discussed in Sec. IV.C? In order to meaningfully address this question one would have to devise a way to perform an adiabatic exchange of such particles. This is not possible in a strictly 1D geometry but can be done in a Y- or T-junction illustrated in Fig. 13c if one can additionally find a way to shuttle the particles along the wire. This is in principle possible if one can control the physical parameters in the wire locally and drive its segments in and out of the topological phase. Under these conditions it turns out that Majorana particles in 1D structures obey the same non-Abelian exchange statistics as their 2D cousins. For a TI wire this can be demonstrated simply by realizing that the Majorana end-mode is adiabatically connected to the vortex in the Fu-Kane model. In the case of a semiconductor wire the situation is somewhat more complicated but the non-Abelian exchange statistics has been established by an explicit calculation (Alicea *et al.*, 2011). It would thus appear that all known realizations of Majorana particles in 1D and 2D solid state systems obey non-Abelian exchange statistics described by the same braid group. Whether this is a coincidence or a consequence of some fundamental principle remains to be understood.

IV. PROSPECTS FOR OBSERVATION

A. Prospects in nuclear and particle physics

Processes that violate total lepton number by two units ($\Delta L = 2$) are indicators of Majorana neutrinos. In this section, we consider such processes and their prospects for discovering a Majorana particle. We treat $\beta\beta(0\nu)$ first and in greater detail, as it is the most feasible technique to achieve this goal. Furthermore, the observation of $\beta\beta$ is an unambiguous signature for Majorana neutrinos (Schechter and Valle, 1982). Most of the other Majorana particle searches discussed below would be indicative but not conclusive.

Equation 27 makes it clear that the $\beta\beta(0\nu)$ decay rate is directly related to the Majorana neutrino mass. Table I summarizes the most recent $\beta\beta(0\nu)$ experimental results, which indicate $T_{1/2}^{0\nu}$ is greater than 10^{25} y; more than 10^{15} times longer than the age of the Universe. This long half-life limit constrains the effective Majorana neutrino mass to be very small. Measuring, or placing limits on, such a slow process is possible because Avogadro’s number is so large. Experiments to date have used about 10 moles of isotope, and future proposals will be much larger yet. It is the advantage from monitoring such a large number of atoms that makes $\beta\beta(0\nu)$ the most sensitive technique to search for light Majorana neutrinos. Experiments that use neutrino sources and targets suffer from low event rates due to modest neutrino fluxes and small weak-interaction cross sections, when searching for $\Delta L = 2$ processes. Some accelerator searches for heavy Majorana neutrinos overcome these limitations when resonant interactions are considered. Hence, in certain limited mass regions, accelerator efforts can compete with $\beta\beta(0\nu)$.

1. Double beta decay

Figure 14 shows how the limit on $\langle m_{\beta\beta} \rangle$ has evolved over the years. The limit improves by about a factor of 2 every 6 years. If this trend continues, the inverted-hierarchy goal for the Majorana mass sensitivity below 50 meV should be explored during the coming decade or so. Within the next few years, the presently operating experiments and those due to come online should extend the reach below 100 meV.

Recent Results The EXO-200 experiment is currently taking data at the Waste Isolation Pilot Plant in New Mexico with 175 kg of liquid xenon enriched to 80% in the isotope 136. Both scintillation light from the interaction and ionization energy deposited by the electrons are detected in the xenon. EXO-200 has recently reported a limit on $\beta\beta(0\nu)$ (Albert *et al.*, 2014; Auger *et al.*, 2012). The collaboration is developing a larger version (nEXO) that will try to observe the Ba daughter from the decay in real-time using laser spectroscopy (Danilov *et al.*, 2000).

TABLE I A list of recent $\beta\beta(0\nu)$ experimental results and their 90% confidence level limits on $T_{1/2}^{0\nu}$. The $\langle m_{\beta\beta} \rangle$ limits are those quoted by the authors using the $M_{0\nu}$ of their choice. The result on ^{76}Ge (Agostini *et al.*, 2013) combines data from Ref. (Aalseth *et al.*, 2002; Klapdor-Kleingrothaus *et al.*, 2001).

Isotope	Technique	$T_{1/2}^{0\nu}$	$\langle m_{\beta\beta} \rangle$ (eV)	Reference
^{48}Ca	CaF_2 scint. crystals	$> 5.8 \times 10^{22}$ y	$< 3.5\text{-}22$	(Umehara <i>et al.</i> , 2008)
^{76}Ge	^{enr}Ge det.	$> 3.0 \times 10^{25}$ y	$< (0.2\text{-}0.4)$	(Agostini <i>et al.</i> , 2013)
^{82}Se	Thin metal foils & tracking	$> 3.2 \times 10^{23}$ y	$< (0.94\text{-}1.71)$	(Tretyak <i>et al.</i> , 2011)
^{100}Mo	Thin metal foils & tracking	$> 1.1 \times 10^{24}$ y	$< (0.3\text{-}0.9)$	(Arnold <i>et al.</i> , 2013)
^{116}Cd	$^{116}\text{CdWO}_4$ scint. crystals	$> 1.7 \times 10^{23}$ y	< 1.7	(Danevich <i>et al.</i> , 2003)
^{128}Te	geochemical	$> 7.7 \times 10^{24}$ y	$< (1.1\text{-}1.5)$	(Bernatowicz <i>et al.</i> , 1993)
^{130}Te	TeO_2 bolometers	$> 2.8 \times 10^{24}$ y	$< (0.3\text{-}0.7)$	(Arnaboldi <i>et al.</i> , 2008)
^{136}Xe	Liq. Xe scint.	$> 1.9 \times 10^{25}$ y	$< (0.16\text{-}0.33)$	(Gando <i>et al.</i> , 2013)
^{150}Ne	Thin metal foil within TPC	$> 1.8 \times 10^{22}$ y	N.A.	(Barabash <i>et al.</i> , 2010)

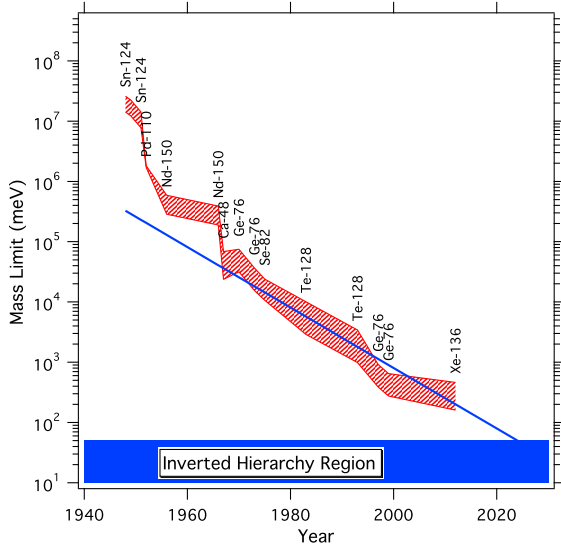


FIG. 14 A history of the effective Majorana neutrino mass limit from $\beta\beta(0\nu)$. The shaded band indicates the range of masses one would deduce from the reported $T_{1/2}^{0\nu}$ as a result of the spread of matrix element calculations. The straight line is an extrapolation drawn by eye for a mass value improvement of a factor of 2 every 6 years. The lower shaded region is the target derived from neutrino oscillation experiments.

The KamLAND-Zen experiment is also searching for $\beta\beta(0\nu)$ in ^{136}Xe . The experiment contains 13 tons of liquid scintillator loaded with 330 kg of Xe enriched to 91% in isotope 136 and operated at the Kamioka mine in Japan. This volume of scintillator is contained with 1000 t of liquid scintillator and 3000 t of mineral oil. The initial results include an improved limit on $\beta\beta(0\nu)$ for ^{136}Xe (Gando *et al.*, 2013). The collaboration has an additional 400 kg of enriched Xe in hand and is considering options to upgrade the detector and reduce backgrounds.

The GERDA experiment, being implemented in two phases, has presented results from high purity Ge detec-

tors enriched in isotope 76 that are operated bare within a large volume of liquid Ar. In Phase 1, about 18 kg of detectors were used, whereas an additional 20 kg will be added for Phase 2. Their first result is a $T_{1/2}^{0\nu} > 3.0 \times 10^{25}$ y when combined with data from previous Ge detector experiments (Agostini *et al.*, 2013).⁶

Near-Term Prospects Several additional experiments should have results by about 2016, including CUORE (Alessandria *et al.*, 2011a), MAJORANA (Abgrall *et al.*, 2013), NEXT (Gómez *et al.*, 2011), SNO+ (Hartnell, 2012), and SuperNEMO (Barabash *et al.*, 2012). Here we briefly describe each.

The CUORE experiment, located at the Gran Sasso National Laboratory in Italy, employs ^{130}Te in the form of natural TeO_2 crystals operated as bolometers. At low temperatures, the heat capacity of these crystals is low enough that the temperature rise due to a radioactive decay can be measured. Therefore, this is a cryogenic setup operated at temperatures around 10 mK. The CUORE detector plans commencing operations in 2014 with 206 kg.

The MAJORANA experiment, like GERDA, uses Ge detectors enriched in isotope 76. (The name of the experiment is in honor of Ettore Majorana.) In this design, the detectors are contained in a more traditional passive high-Z shield constructed of copper and lead. The current phase of MAJORANA will employ 30 kg of Ge enriched to 86% ^{76}Ge and 10 kg of natural Ge detectors. It is being assembled underground at the Sanford Underground Research Facility (SURF) and will have first data in 2014. The MAJORANA Collaboration is planning a ton-scale effort in collaboration with its European counterpart GERDA.

⁶ These 3 results are in tension with an earlier claim (Klapdor-Kleingrothaus and Krivosheina, 2006) for the observation of $\beta\beta(0\nu)$.

NEXT intends to use >100 kg of Xe enriched to $\sim 90\%$ in ^{136}Xe . The detector will be a moderate-density gas TPC, ~ 0.08 g/cm 3 , that will detect scintillation light. By operating at low pressures (~ 15 bar), the design should not only provide good energy resolution, but also permit tracking that allows fairly detailed track reconstruction. It will operate at the Laboratorio Subterráneo de Canfranc, Spain beginning in 2014.

The SNO+ experiment at SNOLAB in Canada plans to fill a large acrylic vessel with liquid scintillator containing dissolved Te. This experiment would also provide a rich physics program of solar neutrino, geoneutrino and supernova neutrino physics.

The SuperNEMO experimental design will use calorimetry to measure energies while using tracking to gather kinematical information about the individual electrons emitted during the decay. It will have a modular design of 20 thin-source planes of 40 mg/cm 2 thickness containing 100 kg of ^{82}Se . A one-module demonstrator with 7 kg of ^{82}Se is planned to be in operation by 2014. The complete experiment will be ready by the end of the decade in an extension of the LSM Modane in the Fréjus Tunnel in France.

Next Generation Efforts The sensitivity goal of the next generation of $\beta\beta(0\nu)$ experiments is to cover the inverted-hierarchy region of Majorana neutrino mass. This region is indicated by other neutrino mass experiments to be between 15 and 50 meV.

For a given experiment, the sensitivity to $\langle m_{\beta\beta} \rangle$ can be written as (Moe, 1991):

$$\langle m_{\beta\beta} \rangle < \frac{(2.50 \times 10^{-5} \text{ meV})}{M_{0\nu}} \sqrt{\frac{NW}{MT f x \epsilon G^{0\nu}}}, \quad (105)$$

where M is the detector mass in kg, T is the live time in years, N is the upper limit on the number of counts assigned to signal, W is the molecular weight of the detector material, f is the isotopic abundance of the $\beta\beta(0\nu)$ isotope, x is the number of $\beta\beta(0\nu)$ atoms per molecule, ϵ is the detection efficiency, and $G^{0\nu}$ is the phase space factor. The constant in the equation has units appropriate for $\langle m_{\beta\beta} \rangle$ given in meV. In most publications, N takes the form of:

$$\begin{aligned} N &= \sqrt{N_B} = \sqrt{b \Delta E M T}, \text{ background limited} \\ &= 1.18, \text{ background free, 68\% CL} \end{aligned} \quad (106)$$

where N_B is the number of background counts, b is the background index or number of background counts per energy and exposure (counts/keV-kg-y), and ΔE is the resolution-determined energy window (referred to as the Region of Interest or ROI) at the endpoint over which the background is measured. The product MT is the exposure, and for an experiment to reach $\langle m_{\beta\beta} \rangle$ sensitivity near 15 meV, requires exposures near 10 t-y and background rates below 1 count/t-y in the region of interest.

The first direct measurement of $\beta\beta(2\nu)$ used a time projection chamber (Elliott *et al.*, 1987). This was a

fairly large apparatus ($\approx \text{m}^3$) for a modest amount of source (13 g) and, therefore, the design doesn't scale easily to large source mass with very low backgrounds. To consider how one might design a large experiment, Eq. 105 can be used to develop a set of criteria for an ideal $\beta\beta(0\nu)$ experiment (Elliott, 2003; Elliott and Vogel, 2002). Such criteria for an experiment to reach the 15 meV goal, include:

- The experimental exposure must be large enough ($MT \approx 10$ t-y). A large quantity of isotope is required and the duty cycle of the experiment must be high. High isotopic abundance in the sample is required, as is a high efficiency of detection.
- The background in the ROI must be low enough ($N_B < 1$ count/t-y).
- Good energy resolution is required to reduce the background rate within the ROI. It is also required to prevent the tail of the $\beta\beta(2\nu)$ spectrum extending into the $\beta\beta(0\nu)$ ROI. Furthermore, good resolution can help prove that a peak is at the expected energy and is therefore due to $\beta\beta(0\nu)$ in the case of an observation.
- A small detector volume minimizes internal backgrounds, when they scale with the detector volume. This is most easily accomplished by an apparatus whose source is also the detector. However, a very large source may have some advantage due to self shielding, although such a configuration may also result in some inefficient use of isotopic material.
- Event reconstruction, providing kinematic data such as opening angle and individual electron energy, can aid in the elimination of backgrounds. This data might also help elucidate the physics if a statistical sample of $\beta\beta(0\nu)$ events is observed.
- Good spatial resolution and timing information can help reject background processes.
- Identifying the daughter in coincidence with the $\beta\beta$ decay energy would eliminate most potential backgrounds except $\beta\beta(2\nu)$.
- The cost of these next generation experiments will be substantial. Therefore, any experiment must be based on a demonstrated technology for the detection of $\beta\beta$. That is, one must demonstrate that one can achieve the required background.
- The nuclear theory is better understood in some isotopes than others. However, arguments have been made (Robertson, 2013) that there is no strongly preferred isotope when all the isotope related factors are considered in Eq. 105.
- A high Q value is desired, as it places the ROI above many potential backgrounds.

No experiment, past or proposed, is able to optimize for all of these characteristics simultaneously. Each collaboration has chosen a design that emphasizes different aspects of this list. In particular, the requirements of a large mass and good energy resolution are frequently at odds. The best resolution experiments use high-purity solid-state detectors (e.g. MAJORANA, GERDA, CUORE). The cost of these detectors impedes instrumenting a large volume. Large quantities of scintillator with dissolved isotope can achieve large masses, but the lack of energy resolution reduces discovery potential (e.g. KamLAND-Zen, SNO+). Table II summarizes the ideas proposed for the future. As can be seen from the number of listings, there are a lot of ideas being pursued (too many to discuss each here, unfortunately).

The most critical feature of any $\beta\beta(0\nu)$ experiment is the background level. All materials have U/Th in trace levels. Typical values are ppm or ppb. If a detector material has Th at a level of 1 ppb, it will have an activity of 10^8 decays per year. For neutrino masses within the inverted-hierarchy region, we expect a $\beta\beta(0\nu)$ decay rate of about 1/t-y or less. Cleaning material to a level that will allow the observation of this low rate is quite a challenge. And even when the technology is available, quality assurance is complicated at this stringent level. At the time of this writing, GERDA has achieved the lowest background in the $\beta\beta(0\nu)$ ROI (Agostini *et al.*, 2013), about 40 counts/(t-y). This is a remarkable achievement but still a factor of 40 above what is required to investigate the inverted hierarchy region.

2. Accelerator Searches

Processes that violate L by 2 units are indicative of the exchange of a virtual Majorana neutrino. When the Majorana neutrino mass is light compared to the energy scale of the process, then the rate of that process will scale as the effective Majorana mass squared ($\langle m \rangle^2 \approx |\sum_{light} U_{ei}^2 m_i|$). This was the possibility discussed in detail for $\beta\beta(0\nu)$ above and given in Eq. 28. In contrast, if the mass is heavy compared to the energy scale, then the rate will scale inversely to the effective Majorana mass ($\langle M \rangle^2 \approx |\sum_{heavy} \frac{V_{ei}^2}{M_i}|$). Such heavy Majorana neutrinos, if they exist, would not only mediate $\beta\beta(0\nu)$, but also processes in high energy collisions at accelerators. In this later case, accelerators can compete with $\beta\beta(0\nu)$ in the search for Majorana fermions under certain conditions.

In Table III, we list frequently searched-for processes that would indicate the existence of Majorana particles. These include: μ to e conversion, meson decay to two leptons, neutrino-antineutrino oscillation, di-lepton production and inverse double beta decay. Neutrinos are not observed in the detectors used to study these processes. Hence they not only carry away missing energy but also lepton number, which can make evidence for a Majorana particle difficult to confirm. Therefore the best limits

come from processes that have lepton number violation but no missing energy.

Atre, Han, Pascoli and Zhang wrote a nice review of the searches for heavy Majorana neutrinos (Atre *et al.*, 2009). A good overview of the field of lepton number conservation including the $\Delta L = 2$ class that is indicative of Majorana neutrinos can be found in the work by de Gouvea and Vogel (de Gouvea and Vogel, 2013). An estimate of the rate of inverse double beta decay $e^-e^- \rightarrow W^-W^-$ is discussed by Rodejohann (Rodejohann, 2011) with a clear discussion of the issue of resonance. This latter reaction is the fundamental $\Delta L = 2$ process.

For heavy Majorana neutrino masses below 5 GeV, meson decays produce good limits. The best are due to $K^+ \rightarrow l^+l^+\pi^-$ (Atre *et al.*, 2009) but only below 350 MeV. For the energies up to 5 GeV, one relies on charm decays from BaBar (Lees *et al.*, 2011) and B decays from BaBar (Lees *et al.*, 2012), CLEO (Edwards *et al.*, 2002), and LHCb (Aaij *et al.*, 2012). Limits on τ decays that provide constraints near 1 GeV were found by Belle (Miyazaki *et al.*, 2013). From 10-100 GeV, past results come from dilepton production in hadron collisions from CDF (Abulencia *et al.*, 2007), DELPHI (Abreu *et al.*, 1997), and L3 (Adriani *et al.*, 1992). The most sensitive $\mu^- \rightarrow e^+$ conversion result comes from the SINDRUM II experiment (Kaulard *et al.*, 1998). None of these results compete with $\beta\beta(0\nu)$ particularly well in constraining the hypothesis of Majorana neutrino exchange.

The hadron collision search is well underway at the LHC. If m_R is near M_W , then the LHC may have sensitivity to Majorana neutrinos in dilepton production, even given the constraints imposed by $\beta\beta(0\nu)$ (Atre *et al.*, 2009). In general, the LHC program will expand the results in energy up to about 500 GeV. The lepton collision technique would be a powerful study from any future linear collider. The reaction $WW \rightarrow ll$ (See Fig. 2) will have a resonant enhancement of its rate when the momentum transfer between the two particles is near that of m_R .

3. Searches for a Fourth Neutrino

There are 3 known neutrino mass eigenstates. Some tantalizing, but as yet not universally accepted, evidence for a fourth neutrino comes from the LSND (Aguilar *et al.*, 2001) and MiniBooNE (Aguilar-Arevalo *et al.*, 2010, 2009) experiments. These experiments are accelerator neutrino oscillation experiments that find their data best described by a neutrino mass difference that does not match that of either the solar or atmospheric oscillation results. Hence, if those results are established, it implies an additional light neutrino state.

When we discussed the see-saw mechanism in Sec. II.B, we focused on the assumption that m_R is very large compared to m_L and m_D . However, if $m_D \gg m_L, m_R$ or if $m_D \approx m_L$ and/or m_R , then the spectrum of neutrino

TABLE II A summary list of the $\beta\beta(0\nu)$ proposals and experiments.

Isotope	Q-Value (MeV)	Technique	Collaborations
^{48}Ca	4.274	CaF_2 scintillating crystals	CANDLES(Umehara <i>et al.</i> , 2008), CARVEL(Zdesenko <i>et al.</i> , 2005)
^{82}Se	2.995	ZnSe scintillating bolometers Thin foils and tracking	LUCIFER(Arnaboldi <i>et al.</i> , 2011) SuperNEMO(Barabash <i>et al.</i> , 2012)
^{76}Ge	2.039	high purity Ge semiconductor detectors	GERDA(Agostini <i>et al.</i> , 2013), MAJORANA(Abgrall <i>et al.</i> , 2013)
^{100}Mo	3.034	CaMoO_4 bolometers Thin foils and tracking ZnMoO_4 bolometers	AMoRE(Lee <i>et al.</i> , 2011) MOON(Ejiri <i>et al.</i> , 2000) Mo Bolometer(Beeman <i>et al.</i> , 2012)
^{116}Cd	2.809	CZT semiconductor detectors	COBRA(Dawson <i>et al.</i> , 2009)
^{130}Te	2.528	TeO_2 bolometers Te dissolved in scintillator	CUORE(Alessandria <i>et al.</i> , 2011a) SNO+(Hartnell, 2012)
^{136}Xe	2.458	liquid Xe time projection chamber Gaseous Xe time projection chamber Xe dissolved in scintillator Scint. liq. Xe within Graphene sphere	EXO-200(Auger <i>et al.</i> , 2012), nEXO, LZ(Akerib <i>et al.</i> , 2013a) NEXT(Gómez <i>et al.</i> , 2011) KamLAND-Zen(Gando <i>et al.</i> , 2013) GraXe(Gómez-Cadenas <i>et al.</i> , 2012)
^{150}Nd	3.371	thin foils and tracking	DCBA(Ishihara <i>et al.</i> , 2000)
^{160}Gd	1.730	$\text{Cd}_2\text{SiO}_5\text{:Ce}$ scint. crystals in liq. scint.	GSO(Wang <i>et al.</i> , 2002)
Various		Quantum dots in liquid scintillator	Quantum Dots(Aberle <i>et al.</i> , 2013; Winslow and Simpson, 2012)

TABLE III A summary $\Delta L = 2$ processes that are studied to search for Majorana neutrinos. These example reactions are just one of many possibilities for each row. For a more detailed discussion, experimental limits rate estimates, and many more such examples, see Refs. (Atre *et al.*, 2009; de Gouvea and Vogel, 2013; Rodejohann, 2011).

Process	Initial L	Final L	Example
Decay	0	2	$\beta\beta(0\nu), K^- \rightarrow \mu^- \mu^- \pi^+$
Conversion	± 1	∓ 1	$\mu^- + (Z, A) \rightarrow e^+ + (Z - 2, A)$
Lepton Decay	± 1	∓ 1	$\tau^- \rightarrow e^+ \pi^- \pi^-$
Lepton Collisions	2	0	$e^- e^- \rightarrow W^- W^-$
Hadron Collisions	0	-2	$pp \rightarrow \mu^+ \mu^+ X$

masses required by the LSND and MiniBooNE results can be accommodated. Hence, the discovery of a fourth neutrino mixing with the 3 known neutrinos would not prove that neutrinos are Majorana, but it does fit that paradigm well.

There are a large number of searches, ongoing and proposed, for a fourth neutrino mass eigenstate. These searches include experiments using neutrinos produced by accelerators, reactors, and intense radioactive sources, as well as observations in astrophysics and cosmology. A detailed summary of these searches, in addition to an overview of the theory, is given by Abazajian *et al.* (Abazajian *et al.*, 2012). That review provides summary tables such as those we have provided here for the other classes of searches. Therefore, we do not provide one ourselves.

4. Dark Matter Searches

Dark matter comprises a large fraction of the Universe's energy density and a dominant fraction of the Universe's matter. The nature of dark matter is not fully understood and a large program is underway to elucidate it. The recent long-range planning process for high energy physics in the US has resulted in a number of nice reviews (Buckley *et al.*, 2013; Cushman *et al.*, 2013; Kusenko *et al.*, 2013) detailing this program, and the review by Schumann (Schumann, 2013) ties the field together well in a short summary. The review by Jungman *et al.* (1996) gives details about SUSY and its relationship to dark matter.

There are many candidates for the dark matter particle, which we will indicate by χ_0 , and many of these candidates are Majorana in nature. Detecting dark mat-

ter will not, by itself, be a smoking gun that Majorana particles exist, but it would certainly be a key piece of data addressing the question. To accommodate the astrophysical and cosmological data, these particles must be electrically neutral, non-relativistic and stable. There are 3 techniques used to search for these particles, including direct detection, indirect detection, and colliding beam experiments. We will discuss these 3 approaches in turn and provide a reference summary of the experimental efforts in Table IV.

Direct detection searches hope to observe Weakly Interacting Massive Particles (WIMP) by their interaction within a low-background particle detector located deep underground. Supersymmetry allows the existence of a particle (the neutralino) whose mass and cross section match well with that required to explain the relic density of dark matter. Furthermore, it would be a Majorana particle. The signature for the resulting reaction

$$\chi_0 + \overset{N}{Z} A \rightarrow \chi_0 + \overset{N}{Z} A, \quad (107)$$

is the recoiling nucleus, which is detected. The recoil energy, however, is low, depositing a few to ten's of keV. Furthermore, the energy spectrum of the recoil is non-descript, being exponentially decreasing. Hence, the detector requirements are stringent with respect to the low energy threshold. Furthermore, the event rate would be very low and, therefore, like $\beta\beta(0\nu)$, the detectors must be very low in background. Seeing a significant signal above background with different targets can provide a consistency test that dark matter is truly being observed. Furthermore, an annual modulation is predicted for the dark matter signal that can help demonstrate its presence. Eventually, directionally sensitive detectors may be able to help confirm that dark matter has been detected.

Space here does not permit a detailed summary of all experiments. Presently, the most sensitive detectors are those based on liquid noble gas targets. The LUX experiment (Akerib *et al.*, 2013b), sited in the Sanford Underground Research Facility, has the best limits on the WIMP detection rate at the time of this writing. It uses liquid Xe as a target and measures the recoil energy through both ionization and scintillation. The combination of these two energy measures permits a separation of the WIMP signal nuclear recoil from background events that produce electron recoils. A water tank shields the Xe from neutrons that might also produce nuclear recoils and, hence, be a serious background. This experiment continues to run.

The XENON experiment is very similar to LUX in concept, although the upcoming target will be a bit larger. It plans to start running in 2015. DEAP will use 3.6 t of liquid Ar within a water shield. It will exploit the difference in timing of scintillation emission between nuclear and electronic recoils to discern background. This project should begin operations in 2014. COUPP is a superheated fluid of CF_3I within a pressure vessel. WIMP interactions create nucleated bubbles that can be iden-

tified optically. An added acoustic signal helps reject background due to α particles. This experiment will start operations imminently.

Indirect detection searches look for processes within astrophysical objects such as

$$\begin{aligned} \chi_0 + \bar{\chi}_0 &\rightarrow q + \bar{q} \\ &\quad l + \bar{l} \\ &\quad W^+ + W^- \\ &\quad Z + Z, \end{aligned} \quad (108)$$

where q represents a quark, W represents a W-boson, and Z represents a Z-Boson. These product particles then decay into particles that can be observed. Heavy astrophysical bodies such as the Sun, dwarf galaxies or the galactic center can gather χ_0 's into a locally high density that enhances the annihilation rate. Satellites looking for anti-particles and experiments searching for high-energy γ rays in the cosmic ray spectrum place limits on this annihilation. The detection scheme for these experiments assumes the particle self annihilates, which is a key characteristic of Majorana particles, such as the neutralino.

The cosmic microwave background multipole spectrum would be modified by dark matter annihilation in the early Universe. The lack of an observed impact on the multipole spectrum leads to significant constraints, especially for low-mass (≈ 10 GeV) WIMP annihilation into electron-positron pairs (Galli *et al.*, 2011).

Collider beam searches look for processes such as

$$q + \bar{q} \rightarrow \chi_0 + \bar{\chi}_0 + X, \quad (109)$$

where the X represents a radiated γ , Z , W or gluon. The χ_0 , being weakly interacting, is not observed within the detector; however, X produces a monojet which is observed. Therefore, the signature is a large missing energy event with a monojet.

B. Observations in solid state devices

As mentioned previously, in the context of condensed matter physics no doubt exists that Majorana fermions should appear in various systems under the right conditions. The theory, which is well understood, provides unambiguous predictions for their occurrence in certain fractional quantum Hall states and in topological superconductors both naturally occurring and artificially engineered. The experimental situation is considerably more fluid with evidence consistent with Majorana fermions existence reported in studies conducted by a number of experimental groups. Although none of the experiments is completely conclusive by itself, taken together they present a compelling case for Majorana fermions in solid state systems. Below we briefly review the key contributions to the worldwide effort to detect Majorana fermions in solid state devices.

TABLE IV A summary list of the dark matter proposals and experiments. Time Projection Chamber is indicated by TPC.

Direct Detection Techniques		
Target	Technique	Collaborations
He	Liquid ^4He	Liquid ^4He (Guo and McKinsey, 2013)
C_xF_y	CF_3I Bubble Chamber	COUPP(Behnke <i>et al.</i> , 2013)
	C_4F_{10} Bubble Chamber	PICO(Crisler <i>et al.</i> , 2013)
	C_3F_8 Bubble Chamber	PICASSO(Archambault <i>et al.</i> , 2012), SIMPLE(Girard <i>et al.</i> , 2012)
CF_4	Gas TPC	DMTPC(Monroe <i>et al.</i> , 2012), DRIFT(Daw <i>et al.</i> , 2011) NEWAGE(Nishimura <i>et al.</i> , 2009), MIMAC(Billard <i>et al.</i> , 2011)
CaWO_4	Scintillating Bolometers	AMORE(Kim, 2011)
CaMoO_4	Scintillating Bolometers	CRESST(Angloher <i>et al.</i> , 2012)
Al_2O_3	Bolometers	ROSEBUD(Cebrian <i>et al.</i> , 2001)
Si	Si Bolometers	SuperCDMS(Agnese <i>et al.</i> , 2013)
	CCD	DAMIC(Barreto <i>et al.</i> , 2012)
Ge	Ge Bolometers	SuperCDMS(Ahmed <i>et al.</i> , 2009),
	Ge Bolometers	EDELWEISS(Armengaud <i>et al.</i> , 2011)
	Ge Diodes	MAJORANA (Abgrall <i>et al.</i> , 2013), CoGeNT(Aalseth <i>et al.</i> , 2013)
	Ge Diodes	TEXONO(Li <i>et al.</i> , 2013), CDEX(Kang <i>et al.</i> , 2013)
Ar	Liquid TPC	DarkSide(Akimov <i>et al.</i> , 2012a), ArDM(Marchionni <i>et al.</i> , 2010)
	Scintillation	MiniCLEAN(Hime, 2011), DEAP(Boulay <i>et al.</i> , 2012)
Ag-Halide	Nuclear Emulsion	Emulsion(Naka <i>et al.</i> , 2013)
NaI	Scintillating Crystals	DAMA/LIBRE(Bernabei <i>et al.</i> , 2012),
		SABRE(Shields <i>et al.</i> , 2013), KIMS-NaI, DM-Ice(Cherwinka <i>et al.</i> , 2012), ANAIS(Amaré <i>et al.</i> , 2012), KamLAND-PICO(Harada <i>et al.</i> , 2012), NAIAD(Alner <i>et al.</i> , 2005)
CsI	Scintillating Crystals	KIMS(Kim <i>et al.</i> , 2012), CINDMS
TeO_2	Bolometer	CUORE(Alessandria <i>et al.</i> , 2011b)
Xe	Gas TPC	NEXT(Gómez <i>et al.</i> , 2011)
	Liquid TPC	LUX(Akerib <i>et al.</i> , 2013b), Zeplin(Akimov <i>et al.</i> , 2012b),
	Liquid TPC	XENON(Aprile <i>et al.</i> , 2012), PandaX(Li <i>et al.</i> , 2012)
	Liquid TPC	LZ(Malling <i>et al.</i> , 2011)
	Scintillator	XMASS(Abe <i>et al.</i> , 2013)
DNA	Suspended Strands	DNA(Drukier <i>et al.</i> , 2012)
Indirect Detection Techniques		
Sun	ν Detection	SuperKamiokande(Tanaka <i>et al.</i> , 2011), HyperK(Abe <i>et al.</i> , 2011) IceCube(Aartsen <i>et al.</i> , 2013), PINGU(Clark <i>et al.</i> , 2012), ANTARES(Adrián-Martínez <i>et al.</i> , 2013)
Galactic Center	γ -ray Detection Antiparticle Detection	Fermi(Ackermann <i>et al.</i> , 2013), PAMELA(Adriani <i>et al.</i> , 2009) AMS(Aguilar <i>et al.</i> , 2013), CALET(Rauch <i>et al.</i> , 2013), GAPS(Hailey, 2009)
Dwarf Spheroidal Galaxies	γ -ray Detection	MAGIC(Aleksić <i>et al.</i> , 2011), HESS(Aharonian <i>et al.</i> , 2008), VERITAS(Geringer-Sameth <i>et al.</i> , 2013), CTA(Acharya <i>et al.</i> , 2013), Fermi(Ackermann <i>et al.</i> , 2013), HAWC(Abeysekara <i>et al.</i> , 2013)
Universe	μ wave Background	WMAP and ACT Data(Galli <i>et al.</i> , 2011)
Collider Techniques		
WIMP Pair Production	Monojet Search	LHC(Mitsou, 2013)

1. Quantum wires and other 1D systems

By far the greatest progress to date in detecting the Majorana zero modes in solid state devices has been achieved in semiconductor quantum wires. Fig. 15a reproduces the original pioneering result of the Delft group (Mourik *et al.*, 2012) showing the historically first experimental evidence for the Majorana zero mode. In the experiment a wire made of an InSb single crystal has been deposited on a substrate equipped with gates and contacted with superconducting and normal metal electrodes as depicted in Fig. 15b. According to the theory explained in Sec. III.C.3 two Majoranas should appear at the ends of the SC sections of the InSb wire. Gates in the substrate are used to deplete the electron density in the section between the SC and normal metal electrodes and thus create a weak link. The existence of the Majorana zero mode is then probed by measuring the tunneling current I through this weak link under an applied voltage bias V . In this setup, to a very good approximation, differential tunneling conductance $g(V) = dI/dV$ is proportional to the density of states in the SC end of the wire adjacent to the tunneling contact. When the magnetic field B is below about 90 mT the tunneling conductance shows a SC gap of about $260\mu\text{eV}$ with no significant features at low energy (Fig. 15a). However, as the field is further increased a zero bias peak is seen to emerge in $g(V)$ which persists until about 400mT and then disappears. This behavior is qualitatively consistent with the theoretical prediction for the Majorana zero mode and has been interpreted as such.

The result described above has been subsequently reproduced by several independent groups (Churchill *et al.*, 2013; Das *et al.*, 2012; Deng *et al.*, 2012; Finck *et al.*, 2013) using variants of the setup indicated in Fig. 15b. In all cases a zero-bias peak has been reported at non-zero magnetic field consistent with the existence of Majorana fermion in this device. These experiments are now viewed as compelling evidence for Majorana particles in quantum wires although it must be noted that zero-bias anomalies often occur in superconducting systems in situations when Majorana fermions are not expected to be present. For instance presence of disorder and multiple bands can conspire to produce zero-bias peaks in semiconductor wires (with the correct magnetic field dependence) even when the system is in the topologically trivial phase (Liu *et al.*, 2012). It is now generally thought that a truly conclusive experiment showing Majorana particles will have to test one of their other unique properties in addition to the zero-bias conductance peak. There exist several proposals in the literature to achieve this. The effects that can be probed include the fractional Josephson effect (Kitaev, 2001), quantized conductance in the ballistic regime (Law *et al.*, 2009; Wimmer *et al.*, 2011), various tests of non-locality (Burnell *et al.*, 2013; Fu, 2010; Nilsson *et al.*, 2008) and the non-Abelian exchange statistics (Alicia *et al.*, 2011). Of these only the first on the list has been thus far tested (Rokhinson *et al.*,

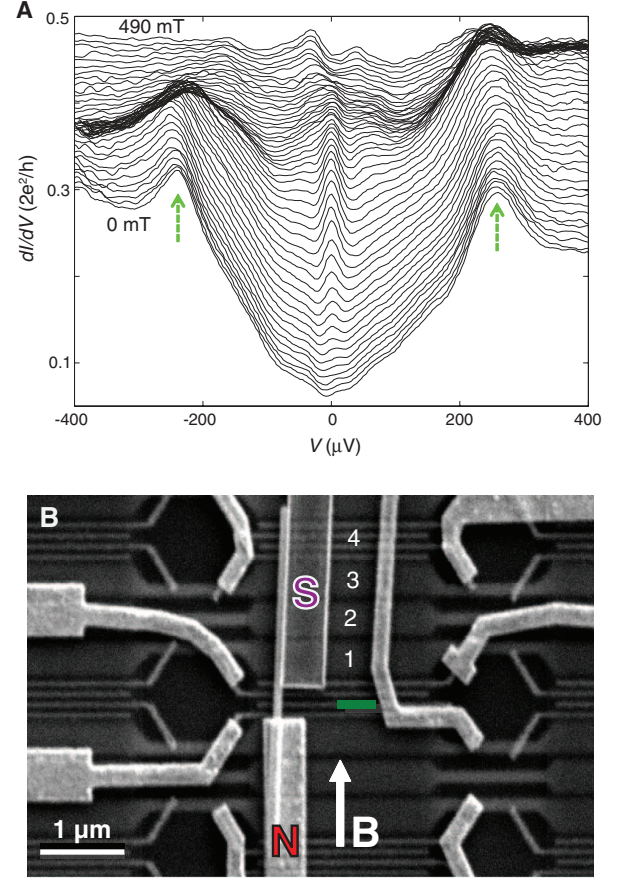


FIG. 15 The Delft experiment [figure adapted from (Mourik *et al.*, 2012)]. a) Tunneling conductance $g(V)$ as a function of the voltage bias showing a SC gap at low magnetic field and the emergence of a zero-bias peak attributed to the Majorana fermion at higher fields. b) Scanning electron microscope image of the device with normal (N) and superconducting (S) contacts attached to an InSb nanowire.

2012) with a positive result. Unfortunately it has been subsequently pointed out that the fractional Josephson effect can actually arise under certain conditions even for Josephson junctions formed of ordinary superconductors with no Majorana zero modes (Sau *et al.*, 2012). At the time of this writing it thus appears that although compelling experimental signatures consistent with Majorana zero modes in semiconductor quantum wires have been observed by multiple groups further experiments will be necessary to obtain truly unambiguous evidence.

Experiments searching for Majorana zero modes in quantum wires made of topological insulators are ongoing but have not yet succeeded in producing evidence. Thus far studies have established the existence of coherent surface states in Bi_2Te_3 nanowires (Peng *et al.*, 2010) and proximity-induced superconducting order has likewise been demonstrated (Zhang *et al.*, 2011). The key obstacle facing the observation of Majorana zero modes appears to be the significant bulk contribution to the

electron conduction. As in the bulk Bi_2Te_3 crystals the chemical potential in wires seems to reside in the bulk valence band. As noted in Sec. III.C.2 topological phase is not expected to arise in this situation. From this vantage point the recently discovered topological insulator $\text{Bi}_2\text{Te}_2\text{Se}$ (Ren *et al.*, 2010) could provide an interesting alternative because at least in crystals the chemical potential is found to reside inside the bulk bandgap. If nanowires of this material can be grown then these should offer a promising platform for Majorana fermions.

Majorana zero modes have not yet been observed in structures based on edge states of 2D topological insulators discussed in Sec. III.C.1. This is chiefly because of the relative paucity of suitable 2D TI materials as well as the notorious difficulty with the fabrication and manipulation of the prototype system, the HgTe quantum well (Franz and Molenkamp, 2013). This proposed realization awaits discovery of new 2D TI materials that are straightforward to grow and fabricate into suitable devices. A worldwide effort to achieve this goal is currently underway (Ezawa, 2012; Knez *et al.*, 2011; Lindner *et al.*, 2011; Liu *et al.*, 2008; Weeks *et al.*, 2011). An innovative proposal has been recently formulated for a reliable transport detection of Majorana zero modes in the edge states of 2D TIs (Mi *et al.*, 2013) which could prove useful if the proposed setup were to be experimentally implemented.

A very recent study (Yazdani, 2010) has reported preliminary evidence for zero-bias peaks (obtained through scanning tunneling spectroscopy) associated with the ends of chains of magnetic Gd atoms deposited on the (110) surface of superconducting Pb crystals. These are consistent with Majorana zero modes discussed in Sec. III.C.4 and if confirmed could constitute an exciting new direction for Majorana research in solid state devices. Potential advantages of these systems include low levels of disorder (since the chain is built on an atomically flat surface one atom at a time) and a possibility to build more complex structures, such as T-junctions and wire networks (Alicia *et al.*, 2011) that will eventually be necessary to manipulate Majorana fermions.

2. 2D systems

The Fu-Kane model discussed in Sec. III.D.2 and its variants remain the focus of experimental efforts in two dimensions. There are two key obstacles that must be overcome in order to implement this proposal. First, for the vortex to contain the Majorana zero mode the chemical potential of the TI must be within its bulk bandgap (or very nearly so). Unfortunately almost all known 3D TIs naturally grow with their chemical potential in their bulk valence or conduction band. Overcoming this problem, which also hampers many other attempts aimed at practical applications of these materials, has been the focus of a worldwide effort and has yielded some promising results (Franz and Molenkamp, 2013). In the setup required by the Fu-Kane model this problem can be further

exacerbated when the TI is interfaced with a superconductor which invariably moves the chemical potential of the surface layer, often in a way that is difficult to predict or control.

The second problem is related to the midgap states associated with the vortex core in the superconductor. The so called Caroli-de Gennes-Matricon states (Caroli *et al.*, 1964) appear at energies $E_n \simeq (\Delta^2/\epsilon_F)(n + 1/2)$ with n integer. Because in typical metallic superconductors $\Delta/\epsilon_F \sim 10^{-3} - 10^{-4}$ the spacing δE of these levels is very small compared to the gap Δ and the vortex core states form essentially a continuum. The Majorana zero mode, if present, is then embedded in this continuum of the vortex core states which makes it difficult or impossible to detect. In addition, because of the proximity of the excited states, such a zero mode is poorly suited for use in quantum information processing. This second problem can be partially overcome by choosing superconductors with larger Δ/ϵ_F ratio and by modifying the basic design e.g. by trapping the vortex in a hole or fabricating a trijunction device proposed in (Fu and Kane, 2008).

The experimental efforts thus far have focused on improving materials and devices with the goal of producing the correct conditions for the emergence of Majorana particles. Superconducting proximity effect has been achieved in surfaces of Bi_2Se_3 with Ti/Al electrodes (Williams *et al.*, 2012) and unconventional Josephson effect possibly indicative of Majorana physics has been reported in these devices. More recently proximity effect in the surface of $\text{Bi}_x\text{Sb}_{2-x}\text{Se}_3$ with chemical potential inside the bulk bandgap has been demonstrated (Cho *et al.*, 2013) paving the way for future detailed studies of Majorana fermions. In addition, high-temperature superconductivity has been induced in Bi_2Se_3 flakes and films by interfacing with a cuprate superconductor $\text{Bi}_2\text{Sr}_2\text{CaCu}_2\text{O}_{8+\delta}$ (Wang *et al.*, 2013.; Zareapour *et al.*, 2012). Very recently, evidence for Majorana zero modes has been reported in the cores of magnetic vortices in a thin film of Bi_2Te_3 grown on the surface of a conventional superconductor NbSe_2 (Xu *et al.*, 2014). Using scanning tunneling spectroscopy some features consistent with the theoretical prediction for the Fu-Kane model (Chiu *et al.*, 2011) have been observed.

V. SUMMARY AND CONCLUSIONS

The concept of Majorana fermion, introduced in the seminal 1937 paper (Majorana, 1937), remains more relevant today than at any previous time. Although experimentally thus far unobserved in the realm of fundamental particles, ongoing searches are now approaching the sensitivity required to test the Majorana character of the leading candidate, the neutrino. In addition, Majorana fermions are thought to play an important role in resolving some of the key outstanding questions in particle physics and cosmology, including leptogenesis (abundance in Universe of matter over antimatter), nature and

origin of the dark matter and the relevance of supersymmetry to our understanding of elementary particles. As discussed in Sec. II supersymmetry requires the existence of superpartners that are Majorana fermions (e.g. the photino, superpartner of the photon). If such particles are stable they may well constitute the dark matter. Similarly, one way to understand the abundance of matter over antimatter in our Universe is through primordial processes involving the decay of heavy Majorana neutrinos accompanied by CP violation in the lepton sector.

Majorana fermions also appear in the formal description of solids with superconducting order. In fact, as argued in Sec. III, quasiparticle excitations above the ground state of any superconductor possess all the key attributes of Majorana fermions: they are electrically neutral spin- $\frac{1}{2}$ fermions indistinguishable from their antiparticles. Of great current interest in solid state physics are Majorana zero modes, i.e. excitations that exist at zero energy and are typically localized and spatially separated from one another. In this situation one can probe their Majorana character in a tabletop experiment and, due to their unusual properties including exotic non-Abelian exchange statistics, even exploit them to perform a protected quantum computation. Compelling experimental evidence exists for Majorana zero modes in semiconductor quantum wires coupled to ordinary superconductors. Their properties are currently a subject of intense experimental and theoretical studies as are other solid state systems that have the potential to harbor Majorana particles.

In more ways than one, Majorana's seminal work may contain clues to our origins. By enabling new transformative technologies it may also pave the way towards our future.

Acknowledgments

We acknowledge support from the Office of Nuclear Physics in the US DOE, Office of Science under grant number LANL20135009 (SRE). We acknowledge support from NSERC and CIFAR (MF). In addition, we are indebted to numerous colleagues for discussions and correspondence that helped shaping our understanding of the subject. Of these, our special thanks go to J. Alicea, C.W.J. Beenakker, A.M. Cook, C.-K. Chiu, T. Goldman, W. Louis, G. Refael and M.M. Vazifeh.

References

- Aaij, R., *et al.*, 2012, Phys. Rev. D **85**, 112004.
Aalseth, C. E., *et al.*, 2002, Phys. Rev. D. **65**, 092007.
Aalseth, C. E., *et al.*, 2013, Phys. Rev. D **88**, 012002.
Aartsen, M. G., *et al.*, 2013, Phys. Rev. Lett. **110**, 131302.
Abazajian, K. N., *et al.*, 2012, summary of the workshop Sterile Neutrinos at the Crossroads, eprint arXiv:1204.5379.
Abe, K., *et al.*, 2011, eprint arXiv:1109.3262.
Abe, K., *et al.*, 2013, eprint arXiv:1301.2815.
Aberle, C., A. Elagin, H. J. Frisch, M. Wetstein, and L. Winslow, 2013, eprint arXiv:1307.5813.
Abeyssekara, A. U., *et al.*, 2013, presented at 33rd International Cosmic Ray Conference, eprint arXiv:1310.0073.
Abgrall, N., *et al.*, 2013, Adv. High Ener. Phys. **2014**, 365432.
Abreu, P., *et al.*, 1997, Z. Phys. C **74**, 57, erratum ibid C 75 (1997) 580.
Abulencia, A., *et al.*, 2007, Phys. Rev. Lett. **98**, 221803.
Acharya, B. S., *et al.*, 2013, Astropart. Phys. **43**, 3.
Ackermann, M., *et al.*, 2013, eprint arXiv:1305.5597.
Adriani, O., *et al.*, 1992, Phys. Lett. B **295**, 371.
Adriani, O., *et al.*, 2009, Nature **458**, 607.
Adrián-Martínez, S., *et al.*, 2013, eprint arXiv:1302.6516.
Agnese, R., *et al.*, 2013, accepted for publication by Phys. Rev. Lett., eprint arXiv:1304.4279.
Agostini, M., *et al.*, 2013, Phys. Rev. Lett. **111**, 122503.
Aguilar, A., *et al.*, 2001, Phys. Rev. D **64**, 112007.
Aguilar, M., *et al.*, 2013, Phys. Rev. Lett. **110**, 141102.
Aguilar-Arevalo, A., *et al.*, 2010, Phys. Rev. Lett. **105**, 181801.
Aguilar-Arevalo, A. A., *et al.*, 2009, Phys. Rev. Lett. **102**, 101802.
Aharonian, F., *et al.*, 2008, Phys. Rev. Lett. **101**, 261104.
Ahmed, Z., *et al.*, 2009, Phys. Rev. Lett. **102**, 011301.
Aitchison, I. J. R., 2009, *Supersymmetry in Particle Physics. An Elementary Introduction* (Cambridge University Press).
Akerib, D. S., *et al.*, 2013a, Nucl. Instrum. Meth. A **704**, 111.
Akerib, D. S., *et al.*, 2013b, eprint arXiv:1310.8214.
Akimov, D., *et al.*, 2012a, eprint arXiv:1204.6218.
Akimov, D., *et al.*, 2012b, Phys. Lett. B **709**, 14.
Albert, J. B., *et al.*, 2014, eprint arXiv:1402.6956.
Aleksić, J., *et al.*, 2011, J. Cosm. Astropart. Phys. **06**, 035.
Alessandria, F., *et al.*, 2011a, submitted to Astropart. Phys., eprint arXiv:1109.0494.
Alessandria, F., *et al.*, 2011b, submitted to Astropart. Phys., eprint arXiv:1109.0494v2.
Alicea, J., 2010, Phys. Rev. B **81**, 125318.
Alicea, J., 2012, Rep. Prog. Phys. **75**, 076501.
Alicea, J., Y. Oreg, G. Refael, F. von Oppen, and M. Fisher, 2011, Nature Physics **7**, 412.
Alder, G. J., *et al.*, 2005, Phys. Lett. B **616**, 17.
Amaré, J., *et al.*, 2012, J. Phys. Conf. Ser. **375**, 012026.
Anderson, P. W., 1972, Science **177**(4047), 393.
Angloher, G., *et al.*, 2012, Eur. Phys. J. C **72**, 1971.
Aprile, E., *et al.*, 2012, Phys. Rev. Lett. **109**, 181301.
Archambault, S., *et al.*, 2012, Phys. Lett. B **711**, 153.
Armengaud, E., *et al.*, 2011, Phys. Lett. B **702**, 329.
Arnaboldi, C., *et al.*, 2008, Phys. Rev. C **78**, 035502.
Arnaboldi, C., *et al.*, 2011, Astropart. Phys. **34**, 344.
Arnold, R., *et al.*, 2013, eprint arXiv:1311.5695.
Atre, A., T. Han, S. Pascoli, and B. Zhang, 2009, JHEP **05**, 30.
Auger, M., *et al.*, 2012, Phys. Rev. Lett. **109**, 032505.
Balantekin, A. B., and W. C. Haxton, 2013, eprint arXiv:1303.2272.
Barabash, A. S., 2010, Phys. Rev. C **81**, 035501.
Barabash, A. S., *et al.*, 2010, talk at conference on Fundamental Interactions Physics (ITEP, Moscow, November 23-27, 2009), eprint arXiv:1002.2862.
Barabash, A. S., *et al.*, 2012, J. Phys. Conf. Ser. **375**, 042012.
Bardeen, J., L. N. Cooper, and J. R. Schrieffer, 1957, Phys. Rev. **108**, 1175.
Barreto, J., *et al.*, 2012, Phys. Lett. B **711**, 264.
Beeman, J. W., *et al.*, 2012, Phys. Lett. B **710**, 318.

- Beenakker, C., 2013a, *Annu. Rev. Con. Mat. Phys.* **4**, 113.
- Beenakker, C., 2013b, arXiv:1312.2001.
- Behnke, E., *et al.*, 2013, submitted to *Phys. Rev. Lett.*, eprint arXiv:1304.6001.
- Bernabei, R., *et al.*, 2012, *J. Phys. Conf. Ser.* **375**, 012002.
- Bernatowicz, T., *et al.*, 1993, *Phys. Rev. C* **47**, 806.
- Billard, J., F. Mayet, C. Grignon, and D. Santos, 2011, *J. Phys. Conf. Ser.* **309**, 012015.
- Boehm, F., and P. Vogel, 1987, *Physics of Massive Neutrinos* (Cambridge University Press).
- Boulay, M. G., *et al.*, 2012, eprint arXiv:1203.0604.
- Braunecker, B., and P. Simon, 2013, *Phys. Rev. Lett.* **111**, 147202.
- Buchmüller, W., R. Peccei, and T. Yanagida, 2005, *Ann. Rev. Nucl. Part. Sci.* **55**, 311.
- Buckley, J., *et al.*, 2013, eprint arXiv:1310.7040.
- Burnell, F. J., A. Shnirman, and Y. Oreg, 2013, *Phys. Rev. B* **88**, 224507.
- Caroli, C., P. de Gennes, and J. Matricon, 1964, *Phys. Lett.* **9**, 307.
- Carruthers, P. A., 1971, *Spin and isospin in particle physics* (Gordon and Breach, New York).
- Cebrian, S., *et al.*, 2001, *Astropart. Phys.* **15**, 79.
- Chamon, C., R. Jackiw, Y. Nishida, S.-Y. Pi, and L. Santos, 2010, *Phys. Rev. B* **81**, 224515.
- Cherwinka, J., *et al.*, 2012, *Astropart. Phys.* **35**, 749.
- Chiu, C.-K., M. J. Gilbert, and T. L. Hughes, 2011, *Phys. Rev. B* **84**, 144507.
- Cho, S., *et al.*, 2013, *Nature Communications* **4**, 1689.
- Choy, T.-P., J. M. Edge, A. R. Akhmerov, and C. W. J. Beenakker, 2011, *Phys. Rev. B* **84**, 195442.
- Churchill, H. O. H., *et al.*, 2013, *Phys. Rev. B* **87**, 241401.
- Clark, K., *et al.*, 2012, *Nucl. Phys. B Proc. Suppl.* **233**, 223.
- Cook, A., and M. Franz, 2011, *Phys. Rev. B* **84**, 201105.
- Cook, A. M., M. M. Vazifeh, and M. Franz, 2012, *Phys. Rev. B* **86**, 155431.
- Crisler, M. B., *et al.*, 2013, presentation at SNOLAB Future Projects Workshop, 2013.
- Cushman, P., *et al.*, 2013, eprint arXiv:1310.8327.
- Danevich, F. A., *et al.*, 2003, *Phys. Rev. C* **68**, 035501.
- Danilov, M., *et al.*, 2000, *Phys. Lett. B* **480**, 12.
- Das, A., Y. Ronen, Y. Most, Y. Oreg, M. Heiblum, and H. Shtrikman, 2012, *Nature Physics* **8**, 887.
- Davidson, S., E. Nardi, and Y. Nir, 2008, *Phys. Rept.* **466**, 105.
- Daw, E., *et al.*, 2011, eprint arXiv:1110.0222.
- Dawson, J. V., *et al.*, 2009, *Phys. Rev. C* **80**, 025502.
- de Gouvea, A., and P. Vogel, 2013, eprint arXiv:1303.4097.
- Deng, M. T., C. L. Yu, G. Y. Huang, M. Larsson, P. Caroff, and H. Q. Xu, 2012, *Nano Letters* **12**, 6414.
- Di Bari, P., 2012, *Contemporary Physics* **53**, 315.
- Dirac, P. A. M., 1928, *Proc. Roy. Soc. A* **117**, 610.
- Drukier, A., *et al.*, 2012, eprint arXiv:1206.6809.
- Eddington, A. S., 1928, *Proc. R. Soc. Lond. A* **121**, 524.
- Edwards, K., *et al.*, 2002, *Phys. Rev. D* **65**, 111102.
- Ejiri, H., *et al.*, 2000, *Phys. Rev. Lett.* **85**, 2917.
- Elliott, S., 2003, in *Yang Institute for Theoretical Physics meeting Neutrinos and Implications for Physics Beyond the Standard Model*, edited by R. Shrock (World Scientific, New Jersey), pp. 351–365.
- Elliott, S. R., A. A. Hahn, and M. K. Moe, 1987, *Phys. Rev. Lett.* **59**, 2020.
- Elliott, S. R., and P. Vogel, 2002, *Ann. Rev. Nucl. Part. Sci.* **52**, 115.
- Ezawa, M., 2012, *New Journal of Physics* **14**(3), 033003.
- Finck, A. D. K., D. J. Van Harlingen, P. K. Mohseni, K. Jung, and X. Li, 2013, *Phys. Rev. Lett.* **110**, 126406.
- Fogli, G. L., E. Lisi, A. Marrone, D. Montanino, A. Palazzo, and A. M. Rotunno, 2012, eprint arXiv:1205.5254v3.
- Franz, M., and L. Molenkamp, 2013, *Topological Insulators* (Elsevier).
- Fu, L., 2010, *Phys. Rev. Lett.* **104**, 056402.
- Fu, L., and C. L. Kane, 2008, *Phys. Rev. Lett.* **100**, 096407.
- Fu, L., and C. L. Kane, 2009, *Phys. Rev. B* **79**, 161408.
- Fukugita, M., and T. Yanagida, 1986, *Phys. Lett. B* **174**, 45.
- Galli, S., F. Iocco, G. Bertone, and A. Melchiorri, 2011, *Phys. Rev. D* **84**, 027302.
- Gando, A., *et al.*, 2013, *Phys. Rev. Lett.* **110**, 062502.
- Gehman, V. M., and S. R. Elliott, 2007, *J. Phys. G* **34**, 667.
- Gell-Mann, M., *et al.*, 1979, *Supergravity* (Amsterdam: North Holland), page 315.
- Geringer-Sameth, A., *et al.*, 2013, presented at 4th Fermi Symposium, eprint arXiv:1303.1406.
- Girard, T., *et al.*, 2012, *Phys. Rev. Lett.* **108**, 259002.
- Gomes, K., W. Mar, W. Ko, F. Guinea, and H. Manoharan, 2012, *Nature (London)* **483**, 306.
- Gómez, E., *et al.*, 2011, eprint arXiv:1106.3630.
- Gómez-Cadenas, J. J., *et al.*, 2012, *J. Cosmol. Astropart. Phys.* **02**, 037.
- Guo, W., and D. N. McKinsey, 2013, eprint arXiv:1302.0534.
- Hailey, C. J., 2009, *New J. Phys.* **11**, 105022.
- Harada, K., *et al.*, 2012, eprint arXiv:1203.4872.
- Hartnell, J. (SNO+), 2012, *J. Phys. Conf. Ser.* **375**, 042015.
- Hasan, M. Z., and C. L. Kane, 2010, *rev. Mod. Phys.* **82**, 3045.
- Hime, A., 2011, eprint arXiv:1110.1005.
- Holstein, B. R., 2009, *J. Phys. Conf. Ser.* **173**, 012019.
- Ishihara, N., *et al.*, 2000, *Nucl. Instrum. Meth. A* **443**, 101.
- Ivanov, D. A., 2001, *Phys. Rev. Lett.* **86**, 268.
- Jungman, G., M. Kamionkowski, and K. Griest, 1996, *Phys. Rep.* **267**, 195.
- Kallin, C., 2012, *Reports on Progress in Physics* **75**(4), 042501.
- Kang, Ke-Jun., *et al.*, 2013, *Front. Phys.* **8**, 412.
- Kaulard, J., *et al.*, 1998, *Phys. Lett. B* **422**, 334.
- Kayser, B., 1989, *The Physics of Massive Neutrinos* (World Scientific Publishing).
- Kayser, B., and A. S. Goldhaber, 1983, *Phys. Rev. D* **28**, 2341.
- Kim, S. C., *et al.*, 2012, *Phys. Rev. Lett.* **108**, 181301.
- Kim, S. K., 2011, presentation at MEDEX 2011, Prague, Czech Republic, eprint <http://medex11.utef.cvut.cz/talks/Kim.pdf>.
- Kitaev, A., 2001, *Phys. Usp.* **44**, 131.
- Kittel, C., 1987, *Quantum theory of solids* (John Wiley & Sons).
- Klapdor-Kleingrothaus, H. V., and I. V. Krivosheina, 2006, *Mod. Phys. Lett. A* **21**, 1547.
- Klapdor-Kleingrothaus, H. V., *et al.*, 2001, *Eur. Phys. J. A* **12**, 147.
- Klinovaja, J., P. Stano, A. Yazdani, and D. Loss, 2013, *Phys. Rev. Lett.* **111**, 186805.
- Knez, I., R.-R. Du, and G. Sullivan, 2011, *Phys. Rev. Lett.* **107**, 136603.
- Kusenko, A., *et al.*, 2013, eprint arXiv:1310.8642.
- Law, K. T., P. A. Lee, and T. K. Ng, 2009, *Phys. Rev. Lett.* **103**, 237001.
- Lee, S. J., *et al.*, 2011, *Astropart. Phys.* **34**, 732.

- Lees, J., *et al.*, 2011, Phys. Rev. D **84**, 072006.
- Lees, J., *et al.*, 2012, Phys. Rev. D **85**, 071103.
- Li, H. B., *et al.*, 2013, Phys. Rev. Lett. **110**, 261301.
- Li, Z., *et al.*, 2012, JINST **8**, 01002.
- Lindner, N. H., G. Refael, and V. Galitski, 2011, Nature Physics **7**, 490.
- Liu, C., T. L. Hughes, X.-L. Qi, K. Wang, and S.-C. Zhang, 2008, Phys. Rev. Lett. **100**, 236601.
- Liu, J., A. C. Potter, K. T. Law, and P. A. Lee, 2012, Phys. Rev. Lett. **109**, 267002.
- Lutchyn, R. M., J. D. Sau, and S. Das Sarma, 2010, Phys. Rev. Lett. **105**, 077001.
- Majorana, E., 1937, Nuovo Cimento **5**, 171, english Translation: Soryushiron Kenkyu **63**,149 (1981).
- Malling, D. C., *et al.*, 2011, eprint arXiv:1110.0103.
- Marchionni, A., *et al.*, 2010, eprint arXiv:1012.5967.
- Martin, I., and A. F. Morpurgo, 2012, Phys. Rev. B **85**, 144505.
- Mi, S., D. I. Pikulin, M. Wimmer, and C. W. J. Beenakker, 2013, Phys. Rev. B **87**, 241405.
- Mitsou, V. A., 2013, invited review for J. Mod. Phys. A, eprint arXiv:1310.1072.
- Miyazaki, Y., *et al.*, 2013, eprint arXiv:1206.5595.
- Moe, M., 1991, Nucl. Phys. B (Proc. Suppl.) **19**, 158.
- Mohapatra, R. N., and P. B. Pal, 1991, *Massive Neutrinos in Physics and Astrophysics* (World Scientific Publishing).
- Monroe, J., *et al.*, 2012, AIP Conf. Proc. **1441**, 515.
- Moore, G., and N. Read, 1991, Nuclear Physics B **360**(23), 362, ISSN 0550-3213.
- Moore, J., 2010, Nature (London) **464**, 194.
- Mourik, V., K. Zuo, S. M. Frolov, S. R. Plissard, E. P. A. M. Bakkers, and L. P. Kouwenhoven, 2012, Science **336**(6084), 1003.
- Nadj-Perge, S., I. K. Drozdov, B. A. Bernevig, and A. Yazdani, 2013, Phys. Rev. B **88**, 020407.
- Naka, T., *et al.*, 2013, Nucl. Instrum. Meth. A. **718**, 519.
- Nayak, C., S. H. Simon, A. Stern, M. Freedman, and S. Das Sarma, 2008, Rev. Mod. Phys. **80**, 1083.
- Nilsson, J., A. R. Akhmerov, and C. W. J. Beenakker, 2008, Phys. Rev. Lett. **101**, 120403.
- Nishimura, H., *et al.*, 2009, J. Phys. Soc. Jpn. Suppl. A **78**, 218.
- Oreg, Y., G. Refael, and F. von Oppen, 2010, Phys. Rev. Lett. **105**, 177002.
- Ostrovsky, P. M., I. V. Gornyi, and A. D. Mirlin, 2010, Phys. Rev. Lett. **105**, 036803.
- Peng, H., *et al.*, 2010, Nature Materials **9**, 225.
- Pientka, F., L. I. Glazman, and F. von Oppen, 2013, Phys. Rev. B **88**, 155420.
- Pontecorvo, B., 1957, Sov. Phys. JETP **6**, 429.
- Pontecorvo, B., 1958, Sov. Phys. JETP **7**, 172.
- Qi, X.-L., and S.-C. Zhang, 2011, Rev. Mod. Phys. **83**, 1057.
- Rauch, B. F., *et al.*, 2013, AIP Conf. Ser. **1516**, 293.
- Read, N., and D. Green, 2000, Phys. Rev. B **61**, 10267.
- Ren, Z., A. A. Taskin, S. Sasaki, K. Segawa, and Y. Ando, 2010, Phys. Rev. B **82**, 241306.
- Robertson, R. G. H., 2013, Mod. Phys. Lett. A **28**, 1350021.
- Rodejohann, W., 2011, eprint arXiv:1106.1334.
- Rokhinson, L. P., X. Liu, and J. K. Furdyna, 2012, Nature Physics **8**, 795.
- Rosenberg, G., H.-M. Guo, and M. Franz, 2010, Phys. Rev. B **82**, 041104.
- Sakharov, A. D., 1967, JETP Lett. **5**, 24.
- Sau, J. D., E. Berg, and B. Halperin, 2012, arXiv:1206.4596.
- Sau, J. D., R. M. Lutchyn, S. Tewari, and S. Das Sarma, 2010, Phys. Rev. Lett. **104**, 040502.
- Schechter, J., and J. W. F. Valle, 1982, Phys. Rev. D **25**, 2951.
- Schrödinger, E., 1926, Phys. Rev. **28**, 1049.
- Schumann, M., 2013, Dark matter 2013, presentation at the 33rd International Cosmic Ray Conference, eprint arXiv:1310.5217.
- Shiba, H., 1968, Progress of Theoretical Physics **40**(3), 435.
- Shields, E., *et al.*, 2013, presented at TAUP 2013.
- Stanescu, T., and S. Tewari, 2013, J. Phys.: Condens. Matter **25**, 233201.
- Tanaka, T., *et al.*, 2011, Astrophys. J. **742**, 78.
- Tretyak, V., *et al.*, 2011, AIP Conf. Proc. **1417**, 125.
- Umehara, S., *et al.*, 2008, J.Phys.Conf.Ser. **120**, 052053.
- Vazifeh, M. M., and M. Franz, 2013, Phys. Rev. Lett. **111**, 206802.
- Wang, E., *et al.*, 2013., Nature Physics **9**, 621.
- Wang, S. C., H. T. Wong, and M. Fujiwara, 2002, Nucl. Instrum. Meth. A **479**, 498.
- Weeks, C., J. Hu, J. Alicea, M. Franz, and R. Wu, 2011, Phys. Rev. X **1**, 021001.
- Williams, J. R., *et al.*, 2012, Phys. Rev. Lett. **109**, 056803.
- Wimmer, M., A. R. Akhmerov, J. P. Dahlhaus, and C. W. J. Beenakker, 2011, New Journal of Physics **13**(5), 053016.
- Winslow, L., and R. Simpson, 2012, J. Instrum. **7**, P07010.
- Xu, J.-P., *et al.*, 2014, arXiv:1312.7110.
- Yanagida, T., 1979, 1979, Proc. Workshop on Unified Theory and Baryon Number in the Universe (KEK, Tsuuba, Japan).
- Yazdani, A., 2010, Presentation at conference "majorana physics in condensed matter", erice italy.
- Zareapour, P., *et al.*, 2012, Nature Communications **3**, 1056.
- Zdesenko, Yu. G., *et al.*, 2005, Astropart. Phys. **23**, 249.
- Zhang, D., J. Wang, A. M. DaSilva, J. S. Lee, H. R. Gutierrez, M. H. W. Chan, J. Jain, and N. Samarth, 2011, Phys. Rev. B **84**, 165120.
- Zralek, M., 1997, ACTA Phys. Pol. B **28**, 2225.